공학석사학위 논문

Coupled Analysis for 6-DOF Dynamics of UAV and Modified Blade Element Momentum Theory considering Gust and Flight Conditions

비행조건과 돌풍의 영향을 고려한 Blade Element Momentum Theory 와 쿼드로터형 무인 비행체의 동역학 결합 해석

2019 년 2 월

서울대학교 대학원

기계항공공학부

박 선 후

Coupled Analysis for 6-DOF Dynamics of UAV and Modified Blade Element Momentum Theory considering Gust and Flight Conditions

비행조건과 돌풍의 영향을 고려한 Blade Element Momentum Theory 와 쿼드로터형 무인 비행체의 동역학 결합 해석

지도교수 신 상 준

이 논문을 공학석사 학위논문으로 제출함

2019 년 2 월

서울대학교 대학원
기계항공공학부
박 선 후

박선후의 공학석사 학위논문을 인준함

2019 년 2 월

위 원 장 이 관 중 (인)
부위원장 신 상 준 (인)
위 원 박 영 민 (인)

Abstract

Coupled Analysis for 6-DOF Dynamics of UAV and Modified Blade Element Momentum Theory considering Gust and Flight Conditions

SunHoo Park

Department of Mechanical and Aerospace Engineering

The Graduate School

Seoul National University

New industries such as reconnaissance, surveillance, and courier services are attracting attention as demand and supply of unmanned aerial vehicles increase. Accordingly, many related technologies of unmanned aerial vehicles are being developed. Among them, quadrotor unmanned aerial vehicle (UAV), which is the most famous, is widely used. The vision arrival, and departure algorithm, and many other new technologies have been used to facilitate the use of UAV in urban areas, such as courier transportation or reconnaissance. However, there is a high risk of falling due to crosswinds or shear flows between buildings in urban areas.

Therefore, this thesis aims at realistic flight prediction capability by

combination between six degree of freedom flight dynamics and precision aerodynamics while considering gust as significant influencing factor. Transformation procedure into the wind frame is conducted to analyze gust. Hover, forward flight, and climb of an individual rotor are analyzed using the blade element momentum theory (BEMT) considering rigid blade flapping. In addition, coupled analysis between 6-degree-of-freedom (DOF) flight and BEMT is attempted. Reliability of the software, XFOIL, is demonstrated by comparison against CFD. Validation for hover, forward flight, and climb condition is attempted using the present BEMT. The experimental environment for the target UAV and verification for hover are performed. In addition, experimental equipment is designed for the wind tunnel test and the experiment will be performed. Through the dynamic characteristics of the HILS system provided by DJI and the parameter estimation, the present 6 degree of freedom simulation that can estimate the gain of the black box type flight controller is constructed.

Keywords: Quadrotor, Blade Element Momentum Theory, Rigid flapping, Gust, Flight condition, Coupled Analysis

Student Number: 2017-28496

Contents

Page

공학석사학위 논문 1

Abstract 3

Contents 5

List of Tables 7

List of Figures 8

Chpater 1 Introduction 1

1.1 Background and Motivation 1

1.2 Objectives and Thesis Overview 5

Chpater 2 Theoretical Background 6

2.1 Modified Blade Element Momentum Theory 6

2.1.1 Lift and Drag aerodynamic coefficient table 10

2.1.2 Frame Transformation 14

2.1.3 Aerodynamic Loads Calculation using Blade Element Momentum Theory 20

2.1.4 Blade Element Momentum Theory considering Rigid Blade Flapping 25

2.2 Hybrid Analysis between Blade Element Momentum Theory and Flight Dynamics 29

2.2.1 Quad-rotor Flight Dynamics 29

2.2.2 Coupled Quadrotor Dynamics with Blade Element Momentum

Theory..... 33

2.3 System Identification and Parameter Estimation.....35

Chpater 3 Results 41

3.1 XFOIL Verification.....41

3.2 Blade Element Momentum Theory verification for hover, climb, and forward flight condition.....45

3.3 Coupled Flight Dynamics Simulation Result 59

3.4 Experiment Setting and Result 63

3.4.1 Individual Rotor Thrust Test..... 63

3.4.2 Hardware Simulation in Loop and Experiment setting for Flight Test..... 68

Chpater 4 Conclusion and Future Works 78

4.1 Conclusion.....78

4.2 Future Works 79

Reference 80

국문초록 84

List of Tables

Page

Table 3.1 Blade properties and rotation information at climb conditions 58

Table 3.2 Moment of Inertia(MOI) DJI Matrice 100 [20] 76

Table 3.3 Controller gain (roll) 77

List of Figures

Page

Fig. 1.1 NASA wind tunnel test[8] 3

Fig. 1.2 Computational Aerodynamics of DJI Phantom3[11].....4

Fig. 2.1 Flow model used for momentum theory[14] 8

Fig. 2.2 Visualization images of the wake at various climb, hover, descent speeds[14] 9

Fig. 2.3 XFOIL panel method 12

Fig. 2.4 Chord length of DJI 1345T CW propeller 13

Fig. 2.5 Body frame notation based on gust wind velocity in the body frame16

Fig. 2.6 Body frame notation based on the relative motion 17

Fig. 2.7 Hub and blade frame transformation 18

Fig. 2.8 Top view of the hub frame 19

Fig. 2.9 Blade element aerodynamic force.....24

Fig. 2.10 Blade lift distribution for forward flight condition 28

Fig. 2.11 Quadrotor global frame, body frame notation 32

Fig. 2.12 Combination diagram of BEMT and flight dynamics 34

Fig. 2.13 Chirp signal example[19] 39

Fig. 2.14 Engine throttle system parameter estimation example[21].....40

Fig. 3.1 Grid configuration of DJI 1345T clock-wise direction rotating blade (90% span-wise station) 42

Fig. 3.2 Comparison aerodynamic results of XFOIL and CFD (Cp) 43

Fig. 3.3 Comparison aerodynamic results of XFOIL and CFD (CL , CD).....44

Fig. 3.4 Comparison between BEMT and experiment for Graupner 9×5 ...48

Fig. 3.5 Comparison between BEMT and experiment in climb condition for APC 10×5 in CT 49

Fig. 3.6 Comparison between BEMT and experiment in climb condition for APC 10×5 in CP 50

Fig. 3.7 Comparison between BEMT and experiment in climb condition for APC 10×7 in CT 51

Fig. 3.8 Comparison between BEMT and experiment in climb condition for APC 10×7 in CP 52

Fig. 3.9 Comparison of drag for each equivalent hinge offset position 53

Fig. 3.10 Comparison between BEMT and experiment in forward flight for Graupner 9×5 (tilt angle = 0°) 54

Fig. 3.11 Comparison between BEMT and experiment in forward flight for Graupner 9×5 (tilt angle = 30°) 55

Fig. 3.12 Comparison between BEMT and experiment in forward flight for Graupner 9×5 (tilt angle = 60°) 56

Fig. 3.13 Comparison between BEMT and experiment in forward flight for Graupner 9×5(tilt angle = 90°) 57

Fig. 3.14 Response by the altitude and global position input 61

Fig. 3.15 Predicted response due to the gust 62

Fig. 3.16 DJI 1345T CW blade configuration 64

Fig. 3.17 Present static experimental facility 65

Fig. 3.18 Comparison between BEMT and experiment in static condition for

DJI 1345T CW 66

Fig. 3.19 New type facility for wind tunnel test 67

Fig. 3.20 DJI Matrice 100 HILS setup 71

Fig. 3.21 HILS system of DJI 72

Fig. 3.22 Roll dynamics of DJI simulation 73

Fig. 3.23 CIFER estimation result 74

Fig. 3.24 Steady-state estimation result 75

Fig. 3.25 Present coupled simulation flow 76

Fig. 3.26 Roll response 77

Chpater 1

Introduction

1.1 Background and Motivation

As of today, unmanned aerial vehicles (UAVs) are used in many fields such as courier service, reconnaissance surveillance, and aerial photographing. According to such trend, efforts to expand UAV technologies are being made[1-2]. In the case of quadrotors, attitude and position control have been implemented using the six degree of freedom governing equations derived from simplified aerodynamics models [3-4]. In recent years, the research has been conducted on method of flight controllers combined with machine learning[5]. In addition to the application of quadrotor flight, studies have been carried out to verify the aerodynamic characteristics of individual rotor on climb and forward flight condition through wind tunnel tests [6-10] as shown in Fig. 1.1. Recently, the study has been researched to analyze the interference between drone body and drone blades using computational fluid dynamics(CFD)[11] in Fig. 1.2. However, as research on UAVs such as quadrotor progresses, the issue about crash of UAVs has been increased. Among the crash reason, gust and turbulence are the main causes of unmanned aircraft drops. To solve these problems, researchers have been conducted on robust control methods considering maneuver flight or gust [12-13]. However, there are few

investigations for accurate prediction of the rotor characteristics under gust. To solve these problems, it is necessary to predict the aerodynamic characteristics of the rotor. However, there are few cases that have been verified with experiments[6,8,14,15]. In the case of a quad-rotor type UAV, it is necessary to predict the flight stability due to forward flight speed or the drag against the incoming wind. This requires asymmetric lift and drag predictions caused by the blade flapping. And experimental verification of hybrid analysis is rare and its usefulness is still unclear.

Therefore, it is necessary to analyze dynamics of UAV which is affected by the disturbance due to gust and maneuvering.

Fig. 1.1 NASA wind tunnel test[8]

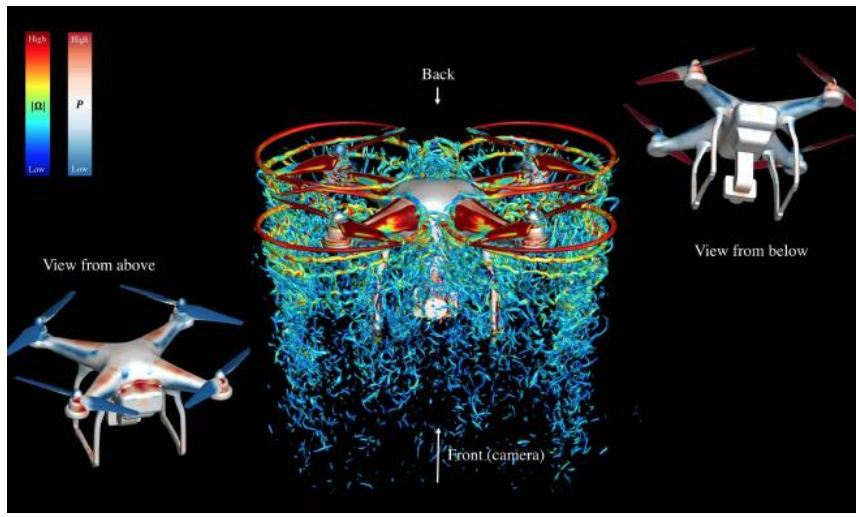

Fig. 1.2 Computational Aerodynamics of DJI Phantom3[11]

1.2 Objectives and Thesis Overview

In this thesis, BEMT considering the gust effect is to be developed[14]. Through the frame transformation from the body frame of a quadrotor to the blade frame of a rotor, the relative wind effect for gust and flight condition is considered. XFOIL is used to obtain aerodynamic result, and reliability of this result is compared against CFD. The derived aerodynamic result is used to verify the experimental values and the present BEMT under hover, ascending, and forward flight conditions. In addition, DJI Matrice 100 is chosen as the target UAV for the coupled analysis between flight dynamics and BEMT. In order to perform it, a static experiment is conducted and compared with the present BEMT. In addition, the hybrid analysis between 6-DOF and the present BEMT is conducted to consider the feasibility of realistic flight simulation. In the case of the target aircraft, DJI M100, the attitude and altitude control are black boxes. Therefore, in order to compare this with the present simulation, the dynamic characteristic of the black box is needed and simplification is needed as a transfer function. In this way, the framework which simulates the precise dynamic characteristics of quadrotor is established.

Chpater 2

Theoretical Background

2.1 Modified Blade Element Momentum Theory

In this section, the concept of modified blade element momentum theory(BEMT)[14] is introduced. BEMT is a combination of blade element theory and momentum theory which is a basic method to analyze rotor aerodynamics because it calculates of the radial and azimuthal aerodynamic load distributions of blade. The momentum theory is using mass and momentum conservation law based of fluid mechanics. The flow model of momentum theory is shown Fig. 2.1, and general governing equations of momentum theory are as follows.

$$\dot{m} = \iint_{\infty} \rho \vec{V} \cdot \overrightarrow{dS} = \iint_{2} \rho \vec{V} \cdot \overrightarrow{dS} \tag{2.1}$$

$$T = \iint_{\infty} \rho(\vec{V} \cdot \overrightarrow{dS})\vec{V} = \dot{m}w \tag{2.2}$$

Then ideal fluid flow assumptions, the simple relationship between induced velocity and slipstream velocity is expressed as Eq. (2.3).

$$v_i = \frac{1}{2}w \tag{2.3}$$

Using this theory, rotor performance can be predicted and induced velocity can be calculated to estimate net force and power of rotor. However, it cannot regard the non-uniform inflow case. For this reason, blade element theory(BET) was first suggested by Drzwiecki. And his study has been an extension of BEMT. Although BEMT is basic rotor analysis, it predicts performance of rotor with relatively accuracy and the computation time is slightly less than Computational Fluid Dynamics (CFD). Thus, in the present aerodynamic load analysis, BEMT is developed and applied.

In this thesis, additional development is carried out to consider the influence of flight conditions, and gust on the basic concept of BEMT. The effect of low Reynolds number is considered because UAV blade is operating under Mach 0.3 conditions. Unlike helicopters, the UAV such as quadrotor uses different shape of airfoil as each radial sections of blade. As each blade airfoil section is different, lift aerodynamic coefficients C_l and drag aerodynamic coefficients C_d are also different from each other. Therefore aerodynamic result of each airfoil section according to the airfoil is required.

In order to consider flight condition, flight working states are regarded. Those are classified State 4 as like normal working state, vortex ring state, turbulent wake state, windmill brake state and is shown Fig. 2.2.

Gust or relative wind of UAV is considered by frame transformation procedure. This process will be introduced later section. The aerodynamic load considering gust and flight condition is estimated by the present BEMT. Furthermore, rigid blade flapping motion for forward flight is regarded.

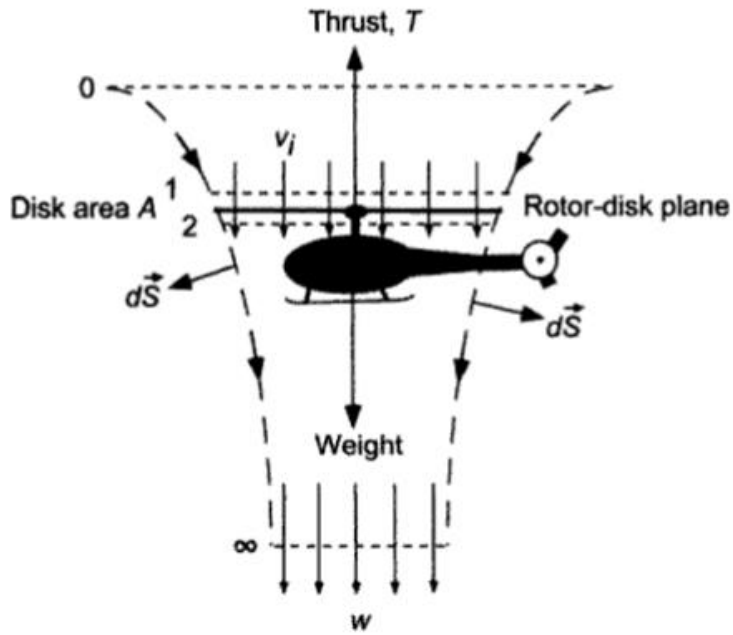

Fig. 2.1 Flow model used for momentum theory[14]

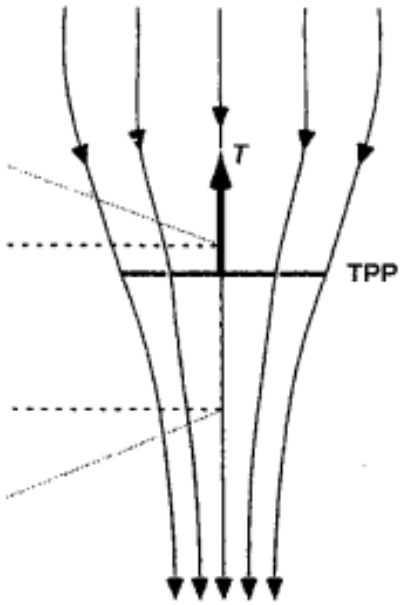

(a) Normal working state

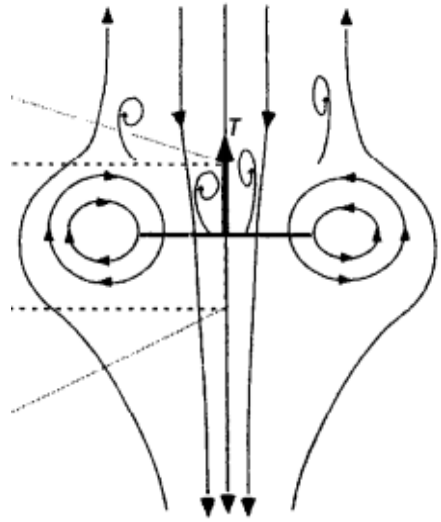

(b) Vortex ring state

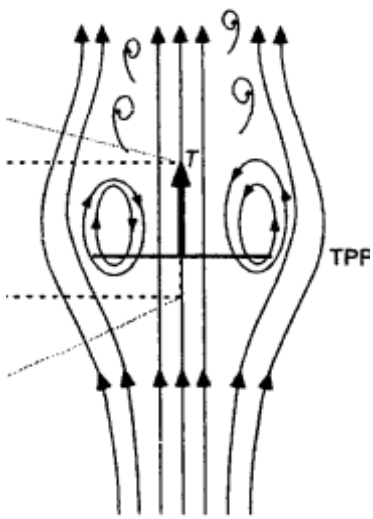

(c) Turbulent wake state

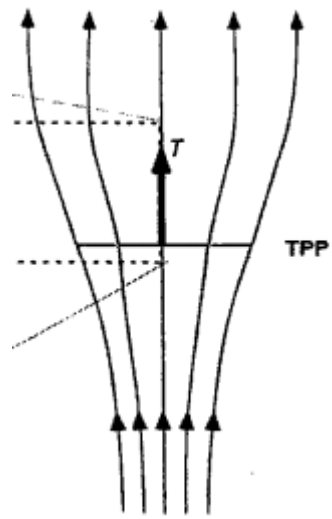

(d) Windmill brake state

Fig. 2.2 Visualization images of the wake at various climb, hover, descent speeds[14]

2.1.1 Lift and Drag aerodynamic coefficient table

The aerodynamic coefficient data of two-dimensional airfoil plays an important role in rotor performance prediction because accuracy of aerodynamic load which is calculated by BEMT is depend on aerodynamic coefficient. Therefore, the accuracy of aerodynamic coefficient data according to the airfoil is necessary.

There are generally three methods for deriving the aerodynamic coefficient of a two-dimensional airfoil. First method is wind tunnel experiment. The target airfoil shape is expanded to three dimensions a wing, and the aerodynamic coefficient according to the angle of attack is derived. Second method is CFD analysis about two-dimensional airfoil. This method is very similar to the experimental results, but it takes a long time to calculate and it is difficult to converge due to the influence of dynamic stall at high angle of attack. Third method is vortex lattice method(VLM). It computes line vortex strength and calculates aerodynamic forces. VLM has relatively short computational time than CFD. But weakness of VLM is inaccurate to compute drag of airfoil in low Reynolds number region which are affected by viscosity effect.

In this study, XFOIL[15] is used for conducting aerodynamic coefficient. There are two reasons for this. First, it is important to obtain aerodynamic coefficient within a short time because the airfoil shape changes in the span direction. Second, although XFOIL is based on VLM, it considers viscosity effect using correlation which referred low Reynolds number experiment trend.

The concept of XFOIL's VLM is shown Fig. 2.3 and governing equation of VLM is as follows.

$$\Psi(x,y) = u_\infty y - v_\infty x + \frac{1}{2\pi}\int \gamma(s)\, ln\, r(s;x,y)\, ds + \frac{1}{2\pi}\int \sigma(s)\, \theta(s;x,y)\, ds \tag{2.4}$$

$$u_\infty = q_\infty cos\alpha,\ u_\infty = q_\infty cos\alpha \tag{2.5}$$

This software requires Reynolds and Mach number as input. Reynolds number can be derived by using Eq. (2.6). Mach number is obtained by substituting the rotation speed, blade radius into Eq. (2.7).

$$Re = \frac{\rho V_\infty c}{\mu} \tag{2.6}$$

$$M = \frac{\Omega R}{a} = \frac{V_\infty}{a} \tag{2.7}$$

μ is dynamic viscosity coefficient, and c is chord length of airfoil as shown in Fig. 2.4. a is speed of sound, and $V_\infty$is velocity of each blade section. Using the above two equations, aerodynamic coefficient table according to Mach and Reynolds number of each section can be constructed. In the validation section, the accuracy of XFOIL are compared and verified by ANSYS Fluent k-ω-SST low Reynolds correction.

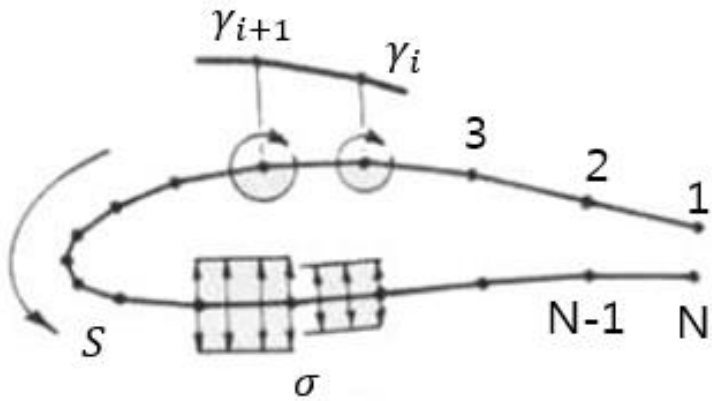

Fig. 2.3 XFOIL panel method

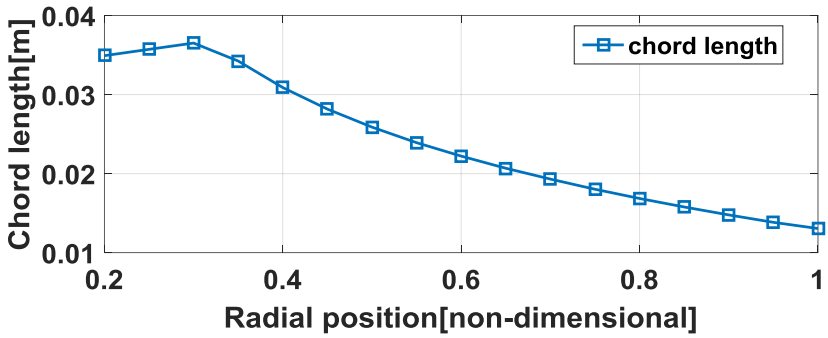

Fig. 2.4 Chord length of DJI 1345T CW propeller

2.1.2 Frame Transformation

In order to consider the inflow for gust and flight condition, it is necessary to clarify the wind velocity in the body frame of the UAV. The velocity of gust or external wind is determined by dividing the direction of $V_x, V_y,$ and V_z axes and it is shown Fig. 2.5. In forward or climb flight conditions case, it can be represented as V_f and V_c, which are the relative velocity of the forward and climb motion. That definition is shown in Fig. 2.6 (a) and (b). The equation is as follows.

$$\begin{bmatrix} U_x \\ U_y \\ U_z \end{bmatrix} = \begin{bmatrix} V_x \\ V_y \\ V_z \end{bmatrix} - \begin{bmatrix} V_f \\ 0 \\ V_c \end{bmatrix} \tag{2.8}$$

The transformation from the body frame to the hub frame of the rotor is derived by the tilt of the roll and pitch directions. As shown in Fig. 2.7 (a) and (b), the roll is expressed by β_r and the pitch is defined by α_p. The expression can be written as follows.

$$\begin{bmatrix} U_{xh} \\ U_{yh} \\ U_{zh} \end{bmatrix} = R_p R_r \begin{bmatrix} U_x \\ U_y \\ U_z \end{bmatrix} \tag{2.9}$$

$$R_p = \begin{bmatrix} cos(\alpha_p) & 0 & -sin(\alpha_p) \\ 0 & 1 & 0 \\ sin(\alpha_p) & 0 & cos(\alpha_p) \end{bmatrix} \tag{2.10}$$

$$R_r = \begin{bmatrix} 1 & 0 & 0 \\ 0 & cos(\beta_r) & sin(\beta_r) \\ 0 & -sin(\beta_r) & cos(\beta_r) \end{bmatrix} \tag{2.11}$$

In this case, R_p is a rotation matrix for α_p, R_r is a rotation matrix for β_r. U_{xh}, U_{yh}, and U_{zh} represent the velocity in the hub frame. The transformation from the hub to the blade frame requires the blade position according to the azimuth angle. Such relationship can be found in Fig. 2.8. The equation can be expressed as follows.

$$\begin{bmatrix} U_{xb} \\ U_{yb} \\ U_{zb} \end{bmatrix} = R_h \begin{bmatrix} U_{xh} \\ U_{yh} \\ U_{zh} \end{bmatrix} \tag{2.12}$$

$$R_h = \begin{bmatrix} cos(\Psi) & sin(\Psi) & 0 \\ -sin(\Psi) & cos(\Psi) & 0 \\ 0 & 0 & 1 \end{bmatrix} \tag{2.13}$$

Ψ is the azimuth angle indicating the blade position in tip path plane. U_{xb}, U_{yb}, and U_{zb} are the blade frame, and R_h is the transformation matrix. Using the frame transformation, forward flight condition and gust can be considered.

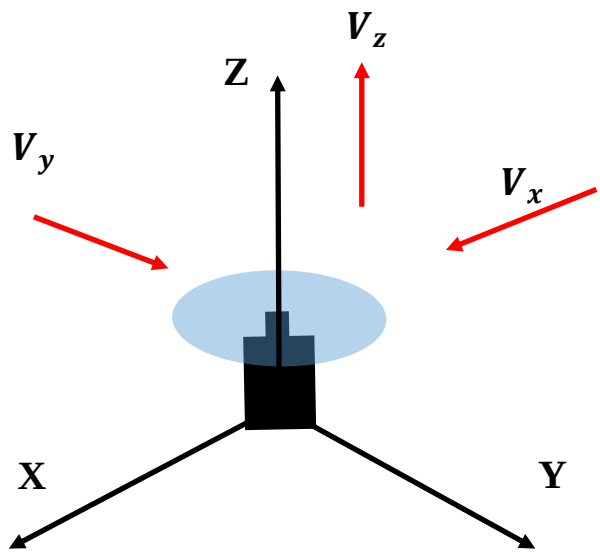

Fig. 2.5 Body frame notation based on gust wind velocity in the body frame

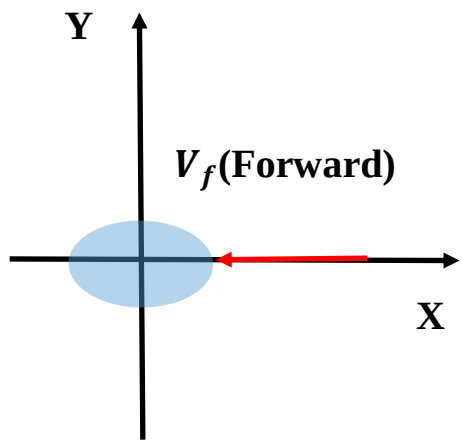

(a) Top view of the body frame

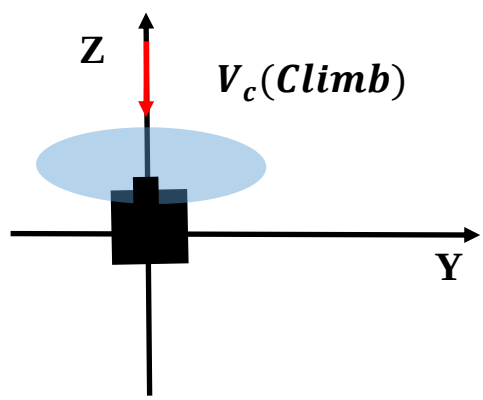

(b) Back view of the body frame

Fig. 2.6 Body frame notation based on the relative motion

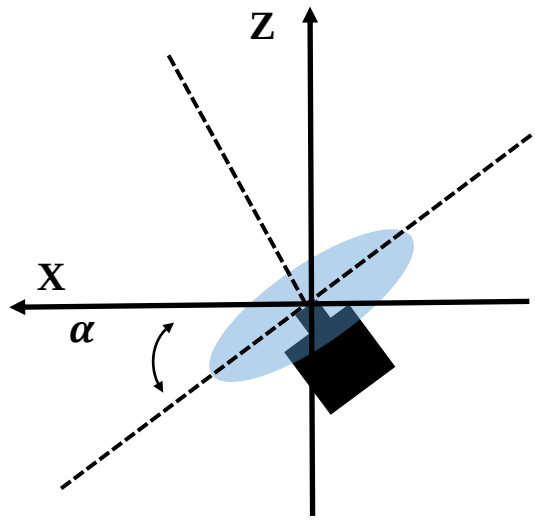

(a) Left side of the rotor

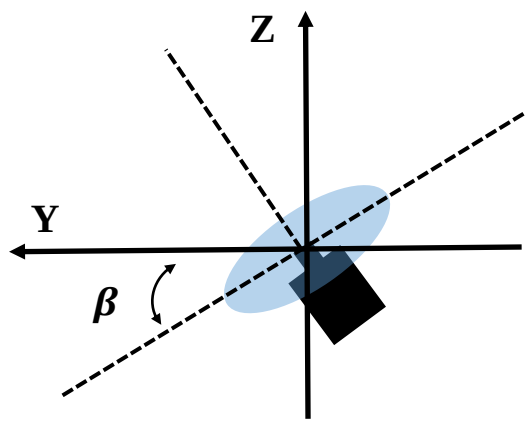

(b) rear side of rotor

Fig. 2.7 Hub and blade frame transformation

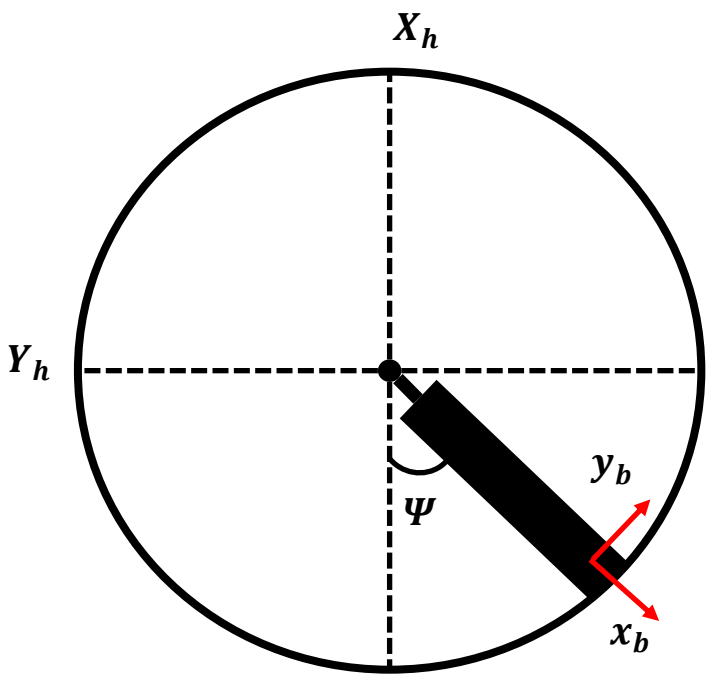

Fig. 2.8 Top view of the hub frame

2.1.3 Aerodynamic Loads Calculation using Blade Element Momentum Theory

BEMT is a combination method between the blade element and momentum theory. The influence of the profile drag cannot be taken into account in the case of the momentum theory. Therefore, BEMT which can analyze more precisely through combination with the blade element theory is used in this thesis. First, as shown in Fig. 2.9 (a), the two-dimensional aerodynamic force can be obtained by the circulation theory. At this time, Eq. (2.14) can be expressed as follows.

$$\begin{bmatrix} U_R \\ U_T \\ U_P \end{bmatrix} = \begin{bmatrix} U_{xb} \\ -U_{yb} + \Omega y \\ -U_{zb} + V_{in} \end{bmatrix} \tag{2.14}$$

V_{in} is induced velocity. In Fig. 2.9 (a), forces acting on airfoil can be expressed sectional normal force, tangential force and moment. Then Eq. (2.15) is obtained and detail of component is defined in Eqs. (2.16) – (2.23).

$$\left.\begin{array}{c} dF_z = dL\cos(\phi) - dDsin(\phi) \\ dF_x = dLsin(\phi) + dDcos(\phi)\cos(\Gamma) \\ dF_r = dDsin(\Gamma) \\ dM_z = dF_x y \end{array}\right\} \tag{2.15}$$

where

$$dL = \frac{1}{2}\rho U_{2d}^2 c(y)(C_l)dy \tag{2.16}$$

$$dD = \frac{1}{2}\rho U_{2d}^2 c(y)(C_d)dy \tag{2.17}$$

$$dM = \frac{1}{2}\rho U_{2d}^2 c^2(y)(C_m)dy \tag{2.18}$$

$$U_{2d} = \sqrt{U_p^2 + U_T^2} \tag{2.19}$$

$$V_{in} = \lambda_i \Omega R \tag{2.20}$$

$$\phi = tan^{-1}(\frac{U_p}{U_T}) \tag{2.21}$$

$$\Gamma = tan^{-1}(\frac{U_R}{U_T}) \tag{2.22}$$

$$\alpha = \theta - \phi \tag{2.23}$$

As shown in Fig. 2.9 (a), U_p and U_T are in-plane velocity components which are perpendicular and tangential direction of an airfoil. $c(y)$ is chord length of the blade element depending on span wise station. U_{2d} is the magnitude of velocity components which are tangential and perpendicular direction velocity, and V_{in} is expressed by inflow ratio multiplied by the rotational speed. Inflow angle ϕ is angle of the wind in the two-dimensional airfoil between U_p and U_T. Γ is the incident yaw angle in radial direction between U_R and U_T. In case of an angle of attack, it is obtained by subtracting the inflow angle from the pitch angle as follows Eq. (2.23). C_l and C_d are obtained through aerodynamic coefficient data which is determined by the angle of attack depending on Mach and Reynolds number. The element lift dL, drag dD are expressed in terms of U_p and U_T.

In Eq. (2.15), inflow ratio can be obtained using Eq. (2.24). This equation is

derived from combination of the momentum and blade element theory to conduct inflow ratio.

$$\left.\begin{array}{c} dC_T = 4F\lambda(\lambda - \lambda_c)rdr \\ dC_T \cong \frac{1}{2}\sigma C_l r^2 dr = \frac{1}{2}\sigma(C_{la}(\theta - \phi) + C_{lb})r^2 dr \end{array}\right\} \quad (2.24)$$

where,

$$F = \begin{cases} \frac{2}{\pi}\cos^{-1}\left(e^{-f_{root}}\right) & when\ r < 0.5 \\ \frac{2}{\pi}\cos^{-1}\left(e^{-f_{tip}}\right) & when\ r > 0.5 \end{cases} \quad (2.25)$$

$$f_{tip} = \frac{N_b}{2}\frac{(1-r)}{r\phi} \quad (2.26)$$

$$f_{root} = \frac{N_b}{2}\frac{r}{(1-r)\phi} \quad (2.27)$$

$$\lambda_c = -\frac{U_z}{\Omega R} = \frac{V_c}{\Omega R} \quad (2.28)$$

$$r = \frac{y}{R} \quad (2.29)$$

$$\sigma(r) = \frac{N_b c(r)}{\pi R} \quad (2.30)$$

F is Prandtl tip loss function, which is defined as a function of loss in blade tip and expressed by root and tip position. N_b is the number of blades and r is the length in the dimensionless span direction. The tip-loss function and hub-loss function have the same value when r is 0.5. Therefore, it is applied as a reference, and when r is between 0.1 and 0.9 except 0, the thrust coefficient and the torque coefficient show an insignificant discrepancy. Conventional method of BEMT usually utilizes symmetric airfoil shape. However, airfoil sections of quadrotor blade are asymmetric shape. For this reason, not only lift

coefficient slope C_{la}, but also lift coefficient offset C_{lb} should be considered. The convergent inflow value is derived by iterating Eq. (2.24) by 2 through 10 times. The force of the rotor in three directions and the moment in three directions are derived as follows. U is reassigned to dL, dD, and dM to estimate the following six-component forces and moments. The six equations, such as T, H, Y, Q, M_x, M_y, are as follows.

$$U = \sqrt{U_p^2 + U_T^2 + U_R^2} \tag{2.31}$$

$$Thrust: T = \frac{N_b}{2\pi}\int_0^{2\pi}\int_0^R dF_z\, d\psi \tag{2.32}$$

$$Drag: H = \frac{N_b}{2\pi}\int_0^{2\pi}\int_0^R (dF_r cos\psi + dF_x sin\psi) d\psi \tag{2.33}$$

$$Side\ force: Y = \frac{N_b}{2\pi}\int_0^{2\pi}\int_0^R (dF_r sin\psi - dF_x cos\psi) d\psi \tag{2.34}$$

$$Torque: Q = \frac{N_b}{2\pi}\int_0^{2\pi}\int_0^R (rdF_x) d\psi \tag{2.35}$$

$$Roll\ moment: M_x = \frac{N_b}{2\pi}\int_0^{2\pi}\int_0^R (dMcos(\psi) + rdF_z sin(\psi)) d\psi \tag{2.36}$$

$$Pitch\ moment: M_y = \frac{N_b}{2\pi}\int_0^{2\pi}\int_0^R (dMsin(\psi) - rdF_z cos(\psi)) d\psi \tag{2.37}$$

By using Eqs. (2.31) – (2.37), gust or external wind effect can be considered, and applied combination analysis of flight dynamics. But, in real flight case, it is necessary to consider the interference between the rotors. For example, in the case of a forward flight, the rear rotor may have a higher rotating rpm because of the interference between the rotors. To consider this relationship, interference factor is applied.

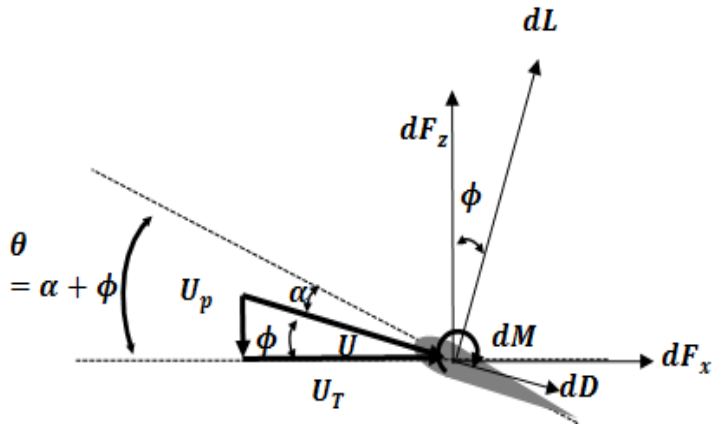

(a) Blade element

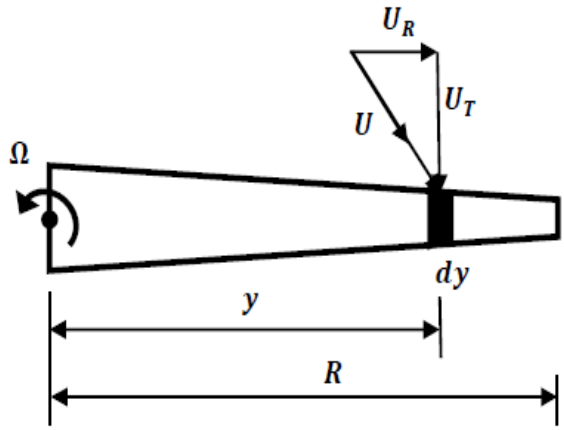

(b) Top view of the blade

Fig. 2.9 Blade element aerodynamic force

2.1.4 Blade Element Momentum Theory considering Rigid Blade Flapping

In case of the rotor system, advancing side and retreating side are generated when the forward flight is performed, so that the asymmetric lift may be induced. It is shown Fig. 2.10. This is the reason why flapping of the blade is created. The drag, side drag, roll, and pitch direction moment are generated. Therefore, it is necessary to precisely predict the aerodynamic forces and moments of the four - component force during forward flight. To consider flapping motion of blade, dF_z, dF_r, U_p in Eqs. (2.14), (2.15) must be modified. This can be expressed as follows.

$$dF_z = (dLcos(\phi) - dDsin(\phi))\cos(\beta_f) \tag{2.38}$$

$$dF_r = -dLsin(\beta_f) + dDsin(\Gamma) \tag{2.39}$$

$$U_P = \lambda\, \Omega\, Rcos(\beta_f) + r\,\dot{\beta}_f + \mu\Omega Rcos(\psi)cos(\beta_f) \tag{2.40}$$

β_f is flapping angle the of the blade and $\dot{\beta}_f$ is the flapping angular velocity. In this case governing equation of the flapping can be written as follows.

$$\frac{\partial^2 \beta_f}{\partial \Psi^2} + \nu_\beta^2 \beta_f = \gamma \overline{M_\beta} + \frac{\omega_{\beta 0}^2}{\Omega}\beta_p \tag{2.41}$$

where,

$$\nu_{\beta_f} = \sqrt{1 + \left(\frac{eS_{\beta_f}}{I_{\beta_f}}\right) + \left(\frac{k_{\beta_f}}{I_{\beta_f}\Omega^2}\right)} = \sqrt{1 + \frac{3}{2}\left(\frac{e}{R}\right) + \frac{\omega_{\beta 0}}{\Omega^2}} \tag{2.42}$$

$$\gamma = \frac{\rho a c R^4}{I_b} \tag{2.43}$$

M_β is the aerodynamic flapping moment, and γ is Lock number. ν_{β_f} is the non-dimensionalized flapping natural frequency. e is the equivalent hinge offset, $\omega_{\beta 0}$ is the non-rotating natural frequency, and $\beta 0$ is the pre-cone angle of flapping. I_b is the moment of inertia at the axis of rotation of the blade and I_{β_f} is the moment of inertia at the hinge. The flapping angle of Eq. (2.41) is related to the pitch angle of blade. The response of flapping blade is assumed as follows with respect to the azimuth angle as in Eq. (2.44).

$$\beta_f(\Psi) = \beta_{0f} + \beta_{1cf} cos(\Psi) + \beta_{1sf} sin(\Psi) \tag{2.44}$$

β_{1cf}, and β_{1sf} are the first order harmonic function coefficient. The first harmonic flap response coefficients β_{0f}, β_{1cf}, β_{1sf} are derived by differential of Eq. (2.44). It is represented as follows.

$$\nu_{\beta_f}^2 \beta_{f0} = \gamma[\frac{\theta_0}{8}(1+\mu^2) + \frac{\theta_{tw}}{10}\left(1 + \frac{5}{6}\mu^2\right) - \frac{\lambda}{6}] \tag{2.45}$$

$$(\nu_{\beta_f}^2 - 1)\beta_{1sf} = \gamma[\frac{1}{8}(-\beta_{1sf})\left(1 + \frac{1}{2}\mu^2\right) - \frac{\mu}{6}\beta_0] \tag{2.46}$$

$$(\nu_{\beta_f}^2 - 1)\beta_{1cf} = \gamma[\frac{1}{8}(\beta_{1cf})\left(1 - \frac{1}{2}\mu^2\right) + \frac{\mu}{3}\theta_0 - \frac{\mu}{4}\lambda + \frac{\mu}{4}\theta_{tw}] \tag{2.47}$$

At this time, due to the difficulty in calculation and the difficulty of obtaining the properties of the blade, the following assumptions is made and carried out. The first assumption is that the blade is a uniform beam. This assumption can be simplified as the formula of Lock number. Second the twist angle of the blade is assumed as the first order linear equation. Third, the slope of the lift coefficient of each airfoil is assumed to be an average data, and the average chord length is also used. Fourth, the blade is assumed to be an equivalent hinge.

Using Eqs. (2.45) – (2.47), flapping angle and flapping angular velocity are conducted. These are applied to Eqs. (2.14), (2.15), and Eqs. (2.38) - (2.40) are conducted.

This flapping consideration can predict more precise forward flight effect of the blade.

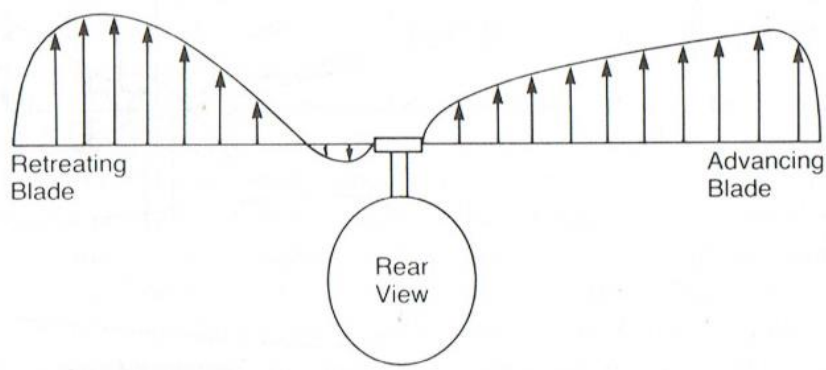

Fig. 2.10 Blade lift distribution for forward flight condition

2.2 Hybrid Analysis between Blade Element Momentum Theory and Flight Dynamics

This section discusses mathematical modeling of the flight dynamics of the quadrotor and introduces the hybrid analysis between BEMT and flight dynamics instead of the highly simplified rotor aerodynamic modeling that has been established in the previous studies[3-4].

2.2.1 Quad-rotor Flight Dynamics

As shown in Fig. 2.11, the flight dynamics of a quadrotor can be expressed as six degrees of freedom of X_g, Y_g, Z_g global frame, X, Y, Z body frame. In case of the body frame, it represents the roll, pitch, and yaw angular rates in term of r_a, p_a, and q_a. The six degrees of freedom equations are expressed as follows.

$$\overline{\dot{V_G}} = \overline{\dot{V_B}} + \overline{\Omega_a} \times \overline{V_B} = \frac{\overline{G_B}}{m} + \frac{\overline{F_{rotor}}}{m} + \frac{\overline{F_{aero-body}}}{m} \tag{2.48}$$

$$\overline{\dot{H_G}} = \overline{\dot{H_B}} + \overline{\Omega_a} \times \overline{H_B} = \overline{M_{rotor}} + \overline{M_{gyro}} \tag{2.49}$$

where,

$$\overline{\Omega_a} = \overline{\omega_b}(body\ fixed) = \begin{bmatrix} p \\ q \\ r \end{bmatrix} \tag{2.50}$$

$$\overline{V_B} = \begin{bmatrix} u \\ v \\ w \end{bmatrix} \tag{2.51}$$

$$\overline{H_B} = \bar{I}\bar{\omega} \tag{2.52}$$

$$\bar{V}_I = \begin{bmatrix} \dot{x_g} \\ \dot{y}_g \\ \dot{z}_g \end{bmatrix} \tag{2.53}$$

The body frame is fixed at the center of gravity of the quadrotor. It suggests that $\bar{\Omega}_a$ is equal to $\overline{\omega_b}$ in the body frame. $\overline{V_B}$ is the velocity of the quadrotor in the body frame, and $\overline{V_G}$ is the velocity of the quadrotor in the global frame. $\overline{G_B}$ represents the gravitational force acting on quadrotor, and $\overline{F_{rotor}}$ is the force in three directions acting on the aircraft. $\overline{H_I}$ is the moment of the UAV in the global frame and $\overline{\mathrm{H_B}}$ is the moment of the body frame. $\overline{M_{rotor}}$ states the moment in three directions acting in the body frame, and $\overline{M_{gyro}}$ is gyroscopic moment induced by the angular velocity of quadrotor. $\overline{J_m}$ is the moment of inertia of the motor. As the motor rotates only in the z direction in the motor frame, $\overline{\omega_{mB}}$ is derived as above. The angle of the quadrotor is expressed by Euler-angle. Euler-angular rate transformation matrix and rotation matrix are as follows.

$$\begin{bmatrix} \dot{\phi_a} \\ \dot{\theta_a} \\ \dot{\psi_a} \end{bmatrix} = \begin{bmatrix} 1 & \mathrm{s}(\phi_a)\,\mathrm{t}(\theta_a) & \mathrm{c}(\phi_a)\,\mathrm{t}(\theta_a) \\ 0 & \mathrm{c}(\phi_a) & -\mathrm{s}(\phi) \\ 0 & \frac{\mathrm{s}(\phi_a)}{\mathrm{c}(\theta_a)} & \frac{\mathrm{c}(\phi_a)}{\mathrm{c}(\theta_a)} \end{bmatrix} \begin{bmatrix} p_a \\ q_a \\ r_a \end{bmatrix} \tag{2.54}$$

$$R_{GB} = \begin{bmatrix} \mathrm{c}(\psi_a)\,\mathrm{c}(\theta_a) & -\mathrm{s}(\psi_a)\,\mathrm{c}(\phi_a) + c(\psi_a)s(\theta_a)s(\phi_a) & \ldots \\ \mathrm{s}(\psi_a)\,\mathrm{c}(\theta_a) & c(\psi_a)c(\phi_a) + s(\psi_a)s(\theta_a)s(\phi_a) & \ldots \\ \mathrm{s}(\theta_a) & c(\theta_a)s(\phi_a) & \ldots \end{bmatrix}$$

$$\begin{bmatrix} s(\psi_a)s(\phi_a) + c(\psi_a)s(\theta_a)\mathrm{c}(\phi_a) \\ -\mathrm{c}(\psi_a)\,\mathrm{s}(\phi_a) + \mathrm{s}(\psi_a)\,\mathrm{s}(\theta_a)\,\mathrm{c}(\phi_a) \\ \mathrm{c}(\theta_a)\,\mathrm{c}(\phi_a) \end{bmatrix} \tag{2.55}$$

ϕ_a, θ_a, and ψ_a are Euler angles, which are derived by integrating the Eq. (2.54). s, c, and t means sin, cos, and tangent, respectively. To facilitate observation, the tilt of the quadrotor is represented by Euler angle, and Eq. (2.55) is multiplied by the rotation matrix.

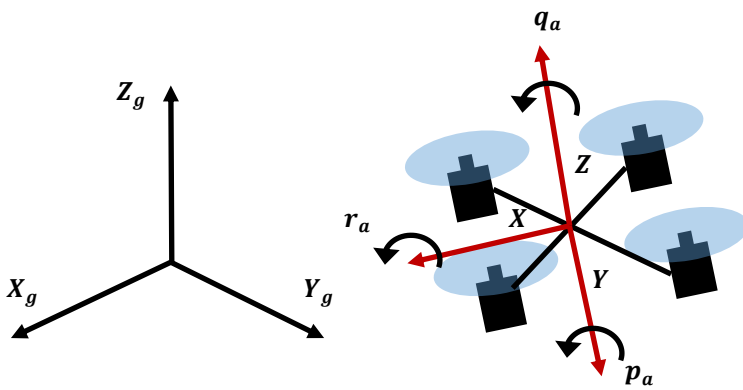

Fig. 2.11 Quadrotor global frame, body frame notation

2.2.2 Coupled Quadrotor Dynamics with Blade Element Momentum Theory

Before describing the coupled analysis between BEMT and the quadrotor, the simplified rotor aerodynamics can be expressed first as in Eq. (2.56).

$$\left.\begin{aligned} T &= \rho\pi R^4\Omega^2 C_T = k_t\Omega^2 \\ Q &= \rho\pi R^5\Omega^2 C_Q = k_q\Omega^2 \end{aligned}\right\} \tag{2.56}$$

Thrust and torque are expressed as a simple hover assumption and uniform inflow. Thus, simplified rotor aerodynamics is not capable of analyzing climb, forward flight, and gust impact. Using the present BEMT, forward, rising flight, and gust can be analyzed. The coupled analysis concept is shown in Fig. 2.12. First, when the rotational speed is input from the rotor, BEMT computes the thrust, torque, drag, and side force using the information of the blade geometry and C81 table, and transfers it to the quadrotor flight dynamics. Then, the information such as climb flight speed, forward flight speed, attitude angle of UAV obtained through flight dynamics is transmitted to BEMT. In addition to this, winds from the outside, such as gusts, can also be considered. By this, 2-way analysis can be performed to simulate the realistic flight.

MATLAB Simulink is used for controller design, and coupled analysis between BEMT and dynamics of quadrotor. The simulation is solved in time domain using 4th order Runge-Kutta method.

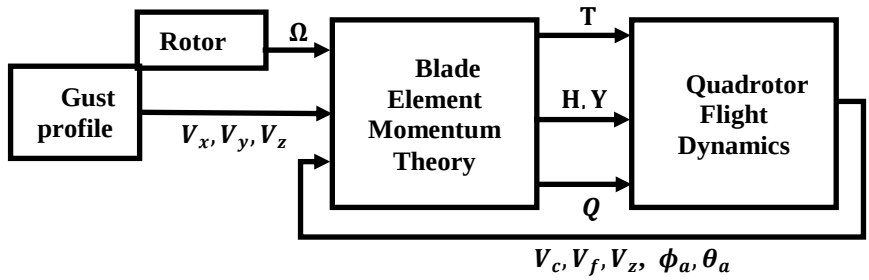

Fig. 2.12 Combination diagram of BEMT and flight dynamics

2.3 System Identification and Parameter Estimation

The definition of system identification is that mathematical model is determined by input and output relationship. In aerospace field, aircraft system identification is a highly efficient method to characterize an aircraft dynamics. However, the identification of dynamics model of flight vehicles from flight-test data is made difficult by many factors[19] such as sensor noise and tightly coupled system of rotorcraft fuselage/rotor/inflow/engine etc. System identification method can be classified two method. The first method is the frequency-response model and second one is the time-response method. The concept of frequency response method is concerned about input/output amplitude and phase ratio. It is useful to identify single-input/single-output (SISO) system such as actuator. However, aircraft and rotorcraft are multi-input/multi-output (MIMO) system. To overcome such weakness, frequency response takes assumptions which make simplify the model of aircraft such as decoupled dynamics or quasi steady aerodynamics cases. On the contrary, time-response is more complicated than frequency response because it need structure of dynamic model for identification. The reason for using the system identification in this study is that the attitude and altitude control algorithm of the target flight vehicle, DJI Matrice 100, is a black box.

In this thesis, since quadrotor dynamic model can be linearized easily, frequency method is adopted. . Among the frequency response methods, the transfer function is derived from two approaches. The first is the chirp signal

method. As shown in Fig. 2.13, the frequency range is varying depend on the time. The input signal equation is as follows.

$$\delta_{sweep} = A_{sweep} sin(\omega_{sweep} t) \tag{2.57}$$

$$\omega_{sweep} = \omega_{sweep_{min}} + K(\omega_{sweep_{max}} - \omega_{sweep_{min}}) \tag{2.58}$$

$$K = C_2[e^{\frac{C_1 t}{T_{sec}}} - 1] \tag{2.58}$$

The first approach is performed by Comprehensive Identification from Frequency Responses(CIFER) program developed by the U.S. army aviation and USRA NASA academic mission services(NAMS).

The second method is similar with first method, but it uses steady-state data amplitude reduction and phase delay of system. This method is performed by MATLAB command 'invfreqs' which finds a continuous-time transfer function that corresponds to a given complex frequency response.

$$H_{TF}(s) = \frac{N(s)}{D(s)} = \frac{b(1)s^n + b(2)s^{n-1} + \cdots + b(n+1)}{a(1)s^m + a(2)s^{m-1} + \cdots + a(m+1)} \tag{2.59}$$

Eq. (2.59) estimates the order of the transfer function by inputting the gain reduction and phase delay of the output frequency according to the input frequency of the system. Algorithm of 'invfreq' uses the weighting least squares method as follows.

$$\min_{b,a} \sum_{k=1}^{n} wt(k)|h(k)A(w(k) - B(w(k))|^2 \quad (2.60)$$

The transfer function of the UAV obtained through the frequency response does not know the inertia moment of the vehicle or the gain of the controller. Therefore, controller gain and related parameters will be derived through coupled simulation using parameter estimation method.

The parameter estimation is based on mathematical model and it optimizes parameters to match measure data and simulation data. An example of parameter estimation can be seen in Fig. 2.14, which minimizes the cost function for the values between the measured data and the simulation data for the engine throttle system. In this thesis, since DJI attitude and altitude controller is a black box, it is necessary to deduce the controller type of the quadrotor and to estimate the parameters for the controller gain.

The controller type is assumed to be PID. And it is composed with angle control which is outer loop of attitude controller and rate control loop which is inner loop of attitude controller. In this case, unlike the classical PID, modified PID is applied so that the system response is less affected by zero. Classical PID and modified PID form are as follows.

$$G_c(t) = K_p \left[e(t) + \frac{1}{\tau_i} \int e(t) + \tau_d \frac{de(t)}{dt} \right] \quad (2.61)$$

$$G_m(t) = K_p \left[\frac{1}{\tau_i} \int e(t) - e(t) - \tau_d \frac{de(t)}{dt} \right] \quad (2.62)$$

Therefore, the cost function is defined for the comparison of the dynamic response between the current simulation and the transfer function derived from the experiment or the reliable simulation, and performs parameter estimation to minimize it. The function 'fmincon' in MATLAB is used for parameter estimation. Cost function is defined as follows.

$$J = \min \sum \left(TF_{output} - O_{present} \right)^2 \tag{2.63}$$

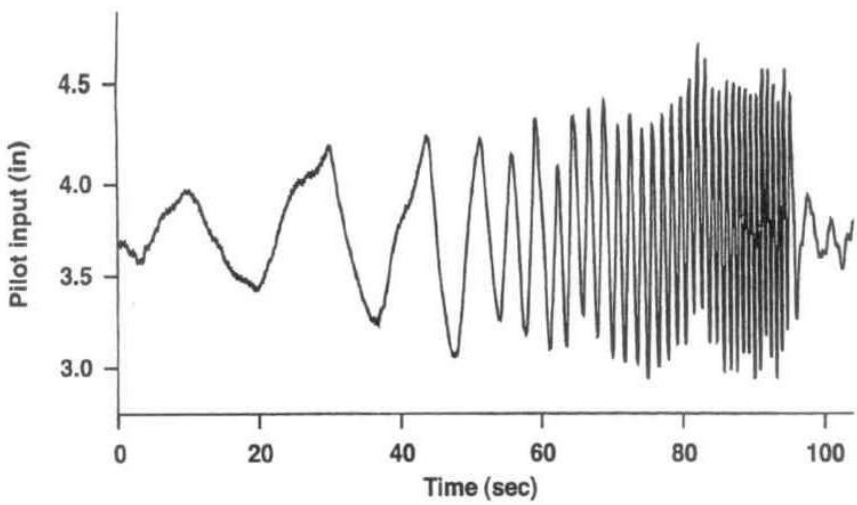

Fig. 2.13 Chirp signal example[19]

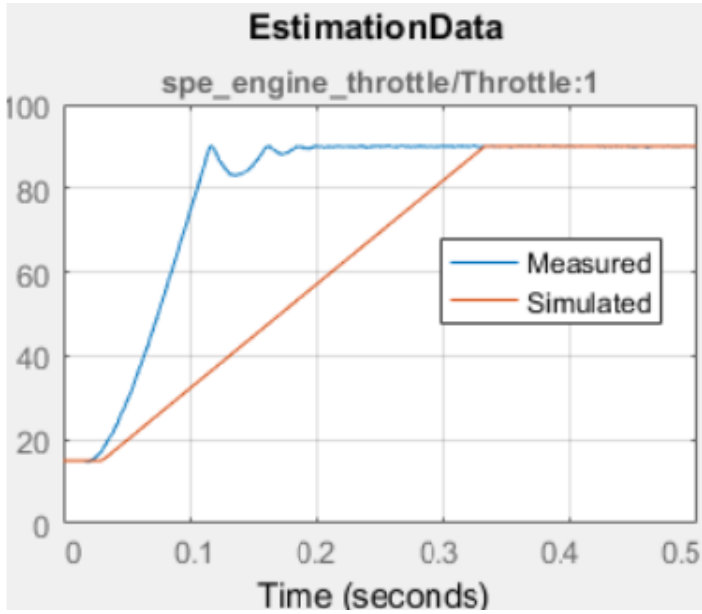

(a) Before parameter estimation iteration

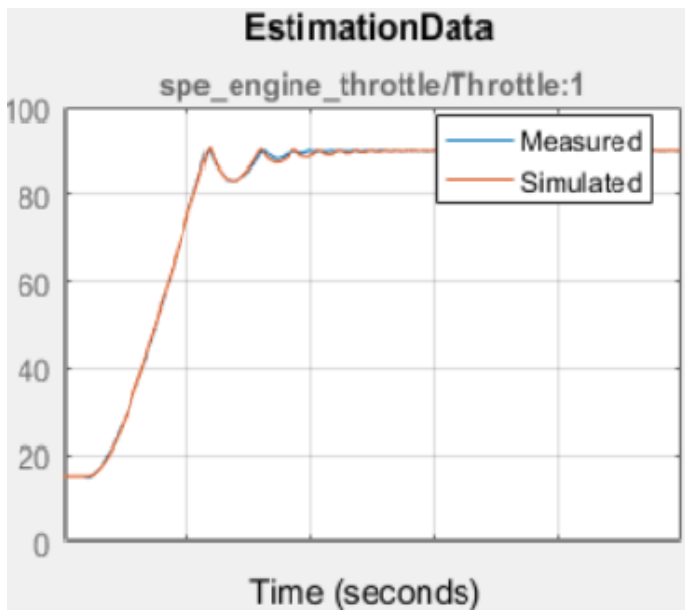

(b) After parameter estimation iteration

Fig. 2.14 Engine throttle system parameter estimation example[21]

Chpater 3

Results

3.1 XFOIL Verification

In the low Reynolds number regime, as the viscosity effect causes a reattached flow to the airfoil, aerodynamic results obtained from XFOIL, which is based on the panel method, needs to be validated. To ascertain the reliability of the aerodynamic results obtained from XFOIL, the verification is performed using ANSYS Fluent k-ω-SST solver considering low Reynolds number correction. The blade is s a DJI 1345T CW, and 90% span direction airfoil is utilized. The entire grids and near airfoil grids are shown in Fig. 3.1, and the total number of nodes is 176,000.

The analysis condition is summarized as follows. Mach number is 0.2, Reynolds number is 6.75×10^4 and the angle of attack is 0, 5, and 10°. In the case of residual, both continuity and energy converged below 10^{-6}.

In Figs. 3.2, and 3.3, C_p distribution, C_L, and C_D according to angle of attack are compared. C_p tends to be almost the same at 0 °, and at 5 ° XFOIL is slightly larger than CFD result. At 10 °, the trend is similar, but result derived from XFOIL are larger than that by CFD. In the case of C_L and C_D, the tendency of coefficient C_D result is similar, but C_L shows that XFOIL predicts larger value than it is by CFD. XFOIL tends to provide larger value

than CFD, but it is considered that that software reflects the viscous effect sufficiently along the trend. Therefore, in this thesis, the cross-sectional aerodynamic results are obtained by use of XFOIL.

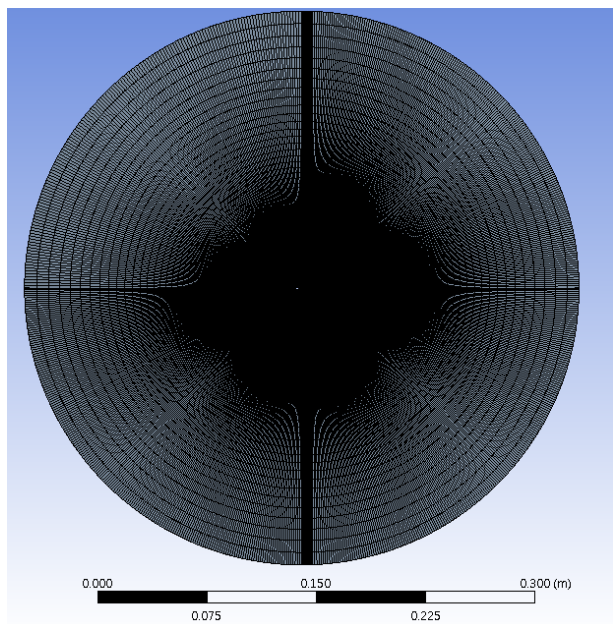

(a) Entire grid configuration

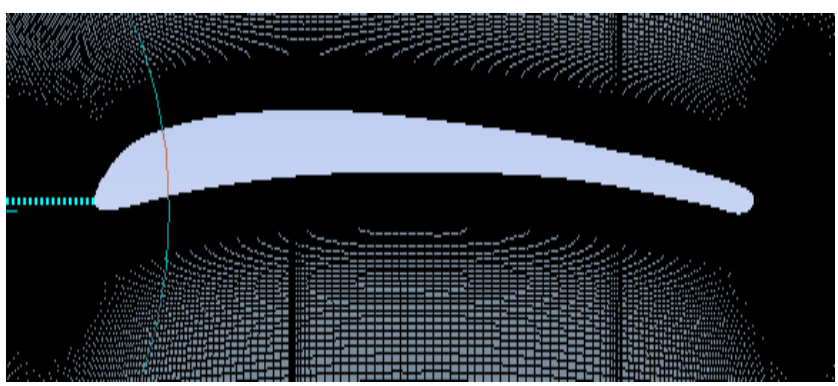

(b) Near airfoil grid

Fig. 3.1 Grid configuration of DJI 1345T clock-wise direction rotating blade (90% span-wise station)

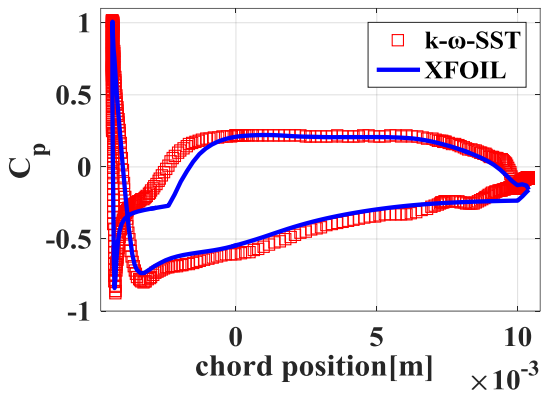

(a) C_p distribution AOA = 0 °

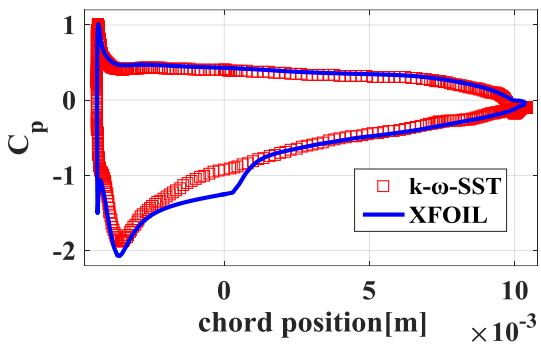

(b) C_p distribution AOA = 5 °

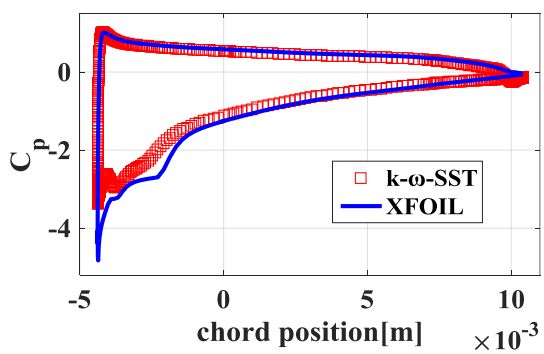

(c) C_p distribution AOA = 10 °

Fig. 3.2 Comparison aerodynamic results of XFOIL and CFD (C_p)

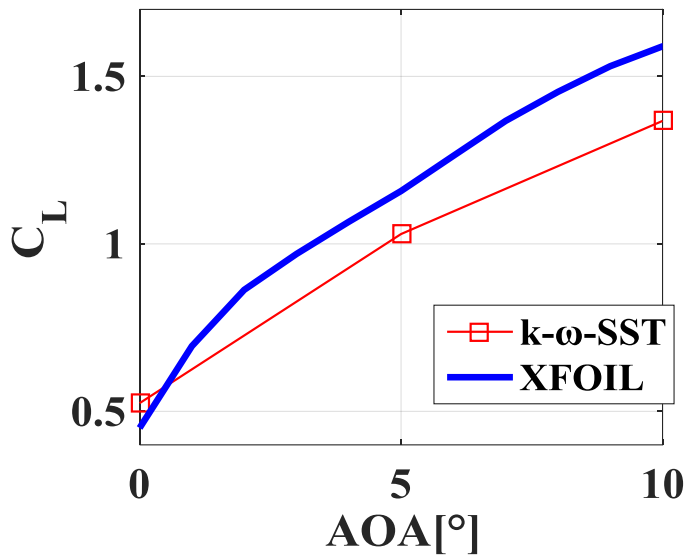

(a) C_L comparison XFOIL

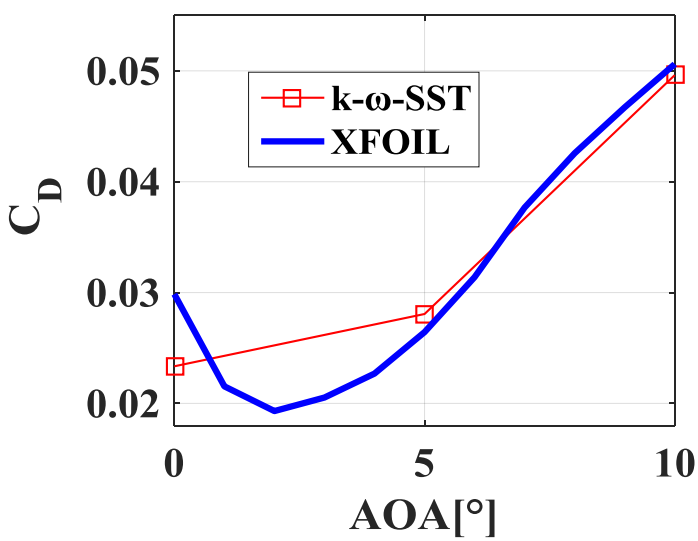

(b) C_D comparison XFOIL

Fig. 3.3 Comparison aerodynamic results of XFOIL and CFD (C_L , C_D)

3.2 Blade Element Momentum Theory verification for hover, climb, and forward flight condition

The present BEMT is executed for the following three conditions: an experiment under hover [6], climb [7], and forward flight condition[6]. Validation of hover and forward flight condition is performed using Graupner 9 × 5 result, as given in Ref.6. APC 10 × 5 and APC 10 × 7 are conducted for climb condition. First, comparison of hover condition about thrust and torque according to RPM is shown in Fig. 3.4. NACA5510 is used, and aerodynamic results are derived from XFOIL. Input RPM range is 2,000 to 10,000. As shown in Fig. 3.4, the results of estimating the hover experimental values of thrust and torque relatively accurately are shown.

In the climb condition, verification is performed using APC 10×5 and APC 10×7 blades. Different cross sections are used for each element in the spanwise direction, as given in Table. 3.1. The wind tunnel results were obtained by Brandt[18]. The horizontal axis in Fig. 3.5, 3.6 represents the vertical advance ratio, μ_z, and the vertical axis expresses either the thrust coefficient C_T or the power coefficient C_P. The variables are derived from the following equations. At this time, the results of climb condition are compared and verified for a rotor rotating at 5,000 and 6,000 RPM.

$$\mu_z = \frac{U_{zb}}{2\Omega R} \tag{3.1}$$

$$C_T = \frac{T}{\rho(2R)^2\left(\Omega_{\mathrm{rpm}}(2\mathrm{R})\right)^2} \tag{3.2}$$

$$C_P = \frac{(2Q_{rpm}\pi)}{\rho(2R)^3\left(\Omega_{\mathrm{rpm}}(2\mathrm{R})\right)^2} \tag{3.3}$$

Fig. 3.5 (a) and (b) compare APC 10 × 5 C_T at 5,000 and 6,000 RPM condition. Fig. 3.6 (a) and (b) compare C_P with experiment result in Ref. 18. The average discrepancy of C_T and C_P is smaller than 10%. In Fig. 3.7,and 3.8, C_T and C_P at 5,000 and 6,000 RPM is compared for APC 10 × 7, and ascertains the tendency. The average discrepancy is smaller than 10%, which indicates that BEMT developed in this thesis well predicts the climb condition.

For forward condition, Graupner 9 × 5 is examined in Ref. 6. The analysis conditions are as follows. The thrust, torque, and drag in the forward direction for the case where the speed of the free stream is 6 m/s and the rotor tilting angles are 0°, 30°, 60°, and 90° are compared. In case of drag, present BEMT considering rigid blade flapping motion and the one performed in Ref. 6 are also compared with experimental results. In this case, the Eq. (2.41) assumes that the non-rotating natural frequency of the blade is 5 Hz because there is no experimental data or reference data of the equivalent hinge offset and the non-rotating natural frequency for derivation of the rotational natural frequency. Also, the blade is assumed to be hingeless and the equivalent hinge offset is analyzed for 2%, 4%, 6%, and 8% blades. To verify the tendency of the location of equivalent hinge offset, it is compared with the present BEMT and experimental result by changing the hinge offset to 2%, 4%, 6%, and 8%, when

the advance angle is 30 °. As shown in Fig. 3.9, The BEMT in Ref. 6, and the present BEMT without the rigid blade flapping show that the discrepancy is increased as high rotational speed. However, the BEMT considering the flapping motion shows good prediction result compared to the experimental result. In this result, flapping motion is affected. The result of Fig. 3.9 is that consideration of the flapping motion in order to simulate precise flight conditions of the quad rotor blades is needed. Also, as shown in Fig. 3.9, when the equivalent offset of the hinge is 2%, the average discrepancy compared to the experimental result is small and the discrepancy is high when the offset is 8%. Therefore, if the forward flight is considered by using accurate values such as the lock number, the moment of inertia of the blade, and the stiffness of the blade derived from the structural test of the actual blade, the result similar to the experimental data will be obtained.

In Figs. 3.10 – 3.14, the thrust and torque show a similar trend compared with the experimental result which is included in Ref. 6. In case of 30°, 60°, 90° except 0°, the tendency and relatively accurate result of drag is obtained.

For the cross-sectional shapes of the blades used in the verification, the same cross-sectional NACA airfoil is used. However, if the three-dimensional scanning is performed to estimate the cross-sectional shape in the span direction in detail, differences in thrust, torque, and drag can be reduced and more accurate results can be obtained than in Figs. 3.10- 3.14

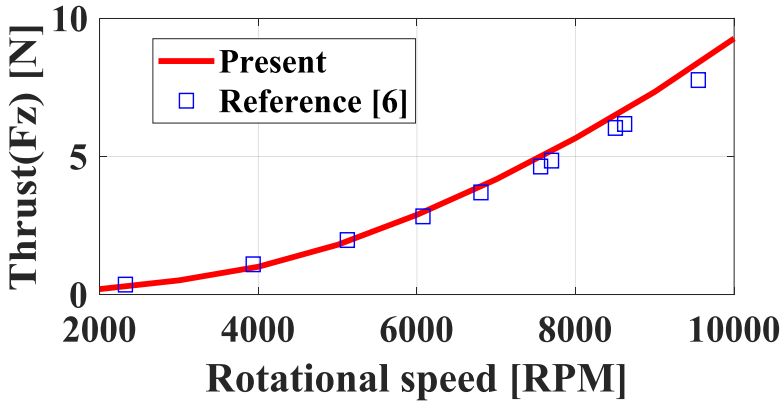

(a) Comparison of BEMT and experiment thrust

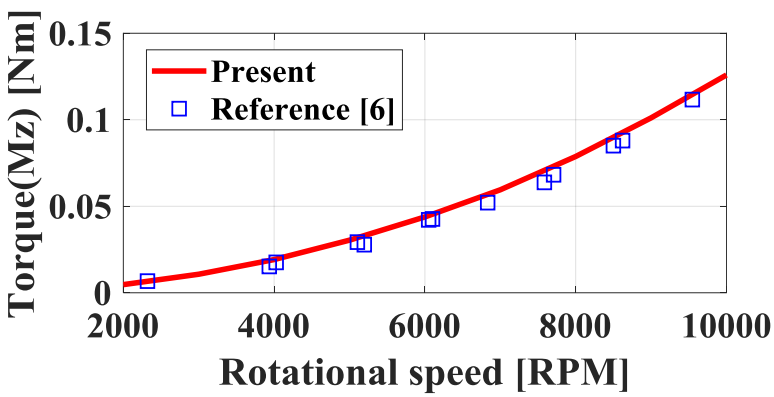

(b) Comparison of BEMT and experiment torque

Fig. 3.4 Comparison between BEMT and experiment for Graupner 9×5

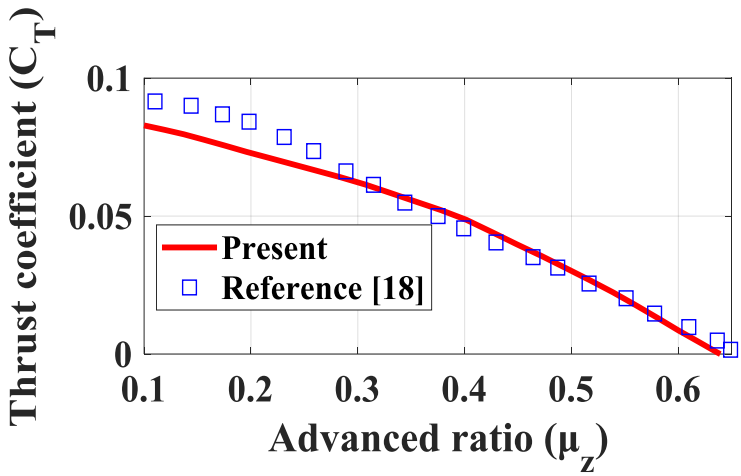

(a) C_T rotating condition – 5,000RPM

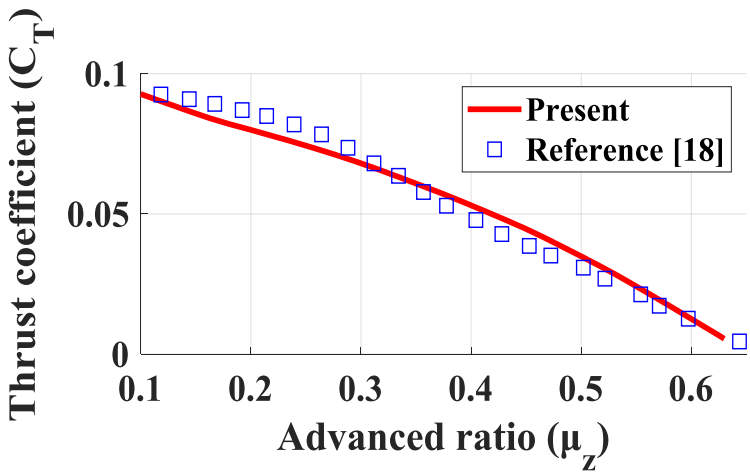

(b) C_T rotating condition – 6,000RPM

Fig. 3.5 Comparison between BEMT and experiment in climb condition for APC 10×5 in C_T

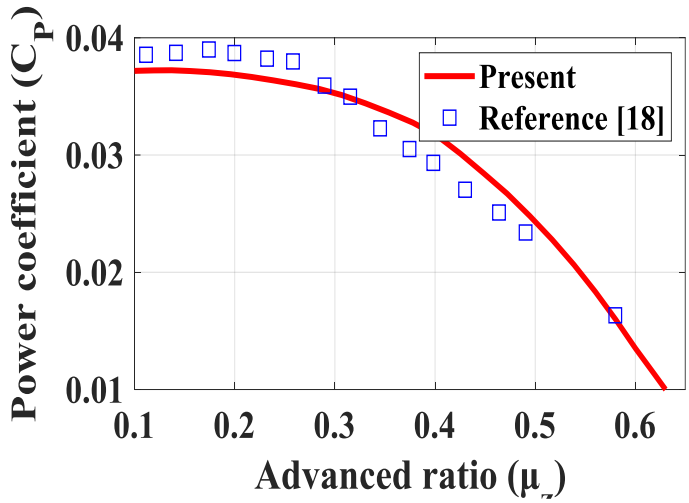

(a) C_P rotating condition – 5,000RPM

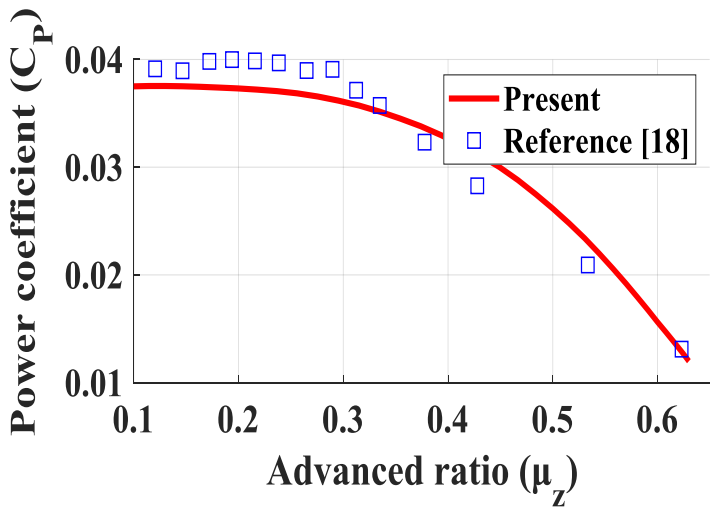

(b) C_P rotating condition – 6,000RPM

Fig. 3.6 Comparison between BEMT and experiment in climb condition for APC 10×5 in C_P

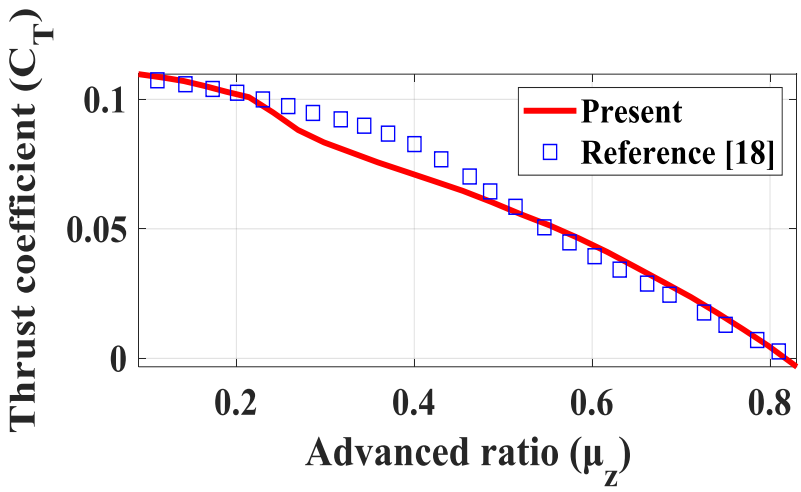

(a) C_T rotating condition – 5,000RPM

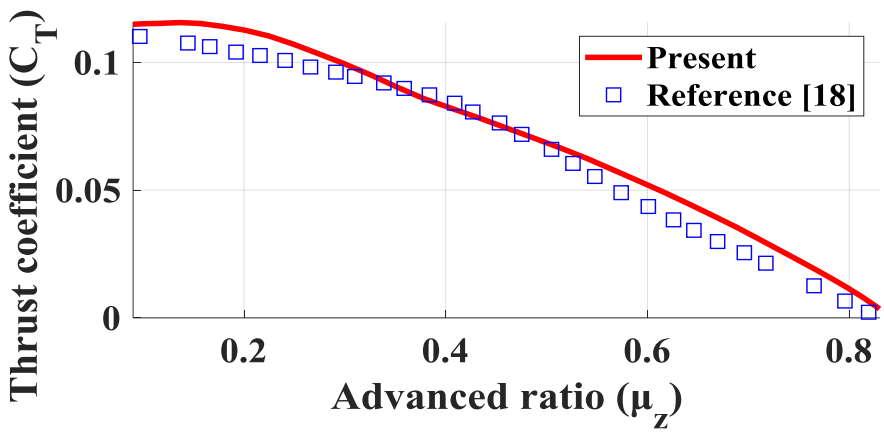

(b) C_T rotating condition – 6,000RPM

Fig. 3.7 Comparison between BEMT and experiment in climb condition for APC 10×7 in C_T

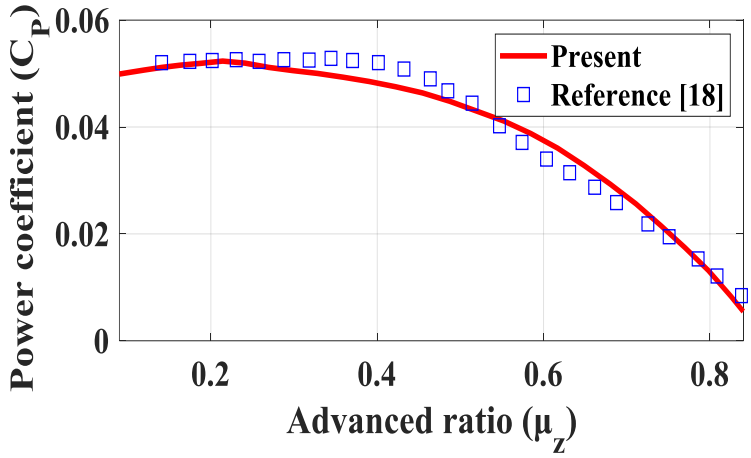

(a) C_P rotating condition – 5,000RPM

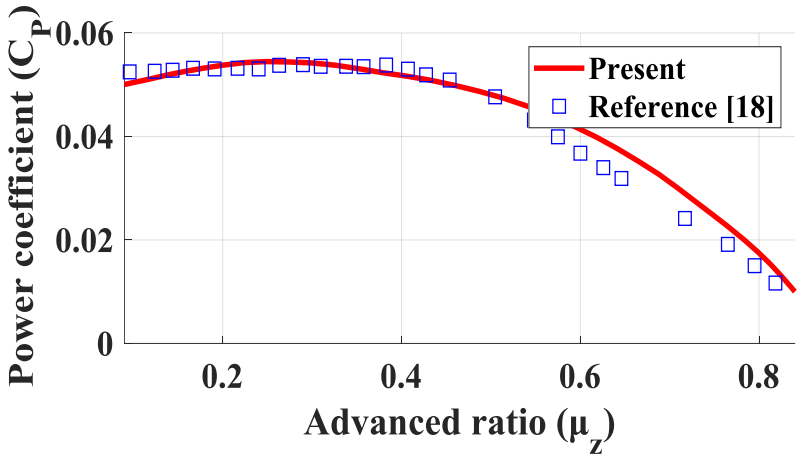

(b) C_P rotating condition – 6,000RPM

Fig. 3.8 Comparison between BEMT and experiment in climb condition for APC 10×7 in C_P

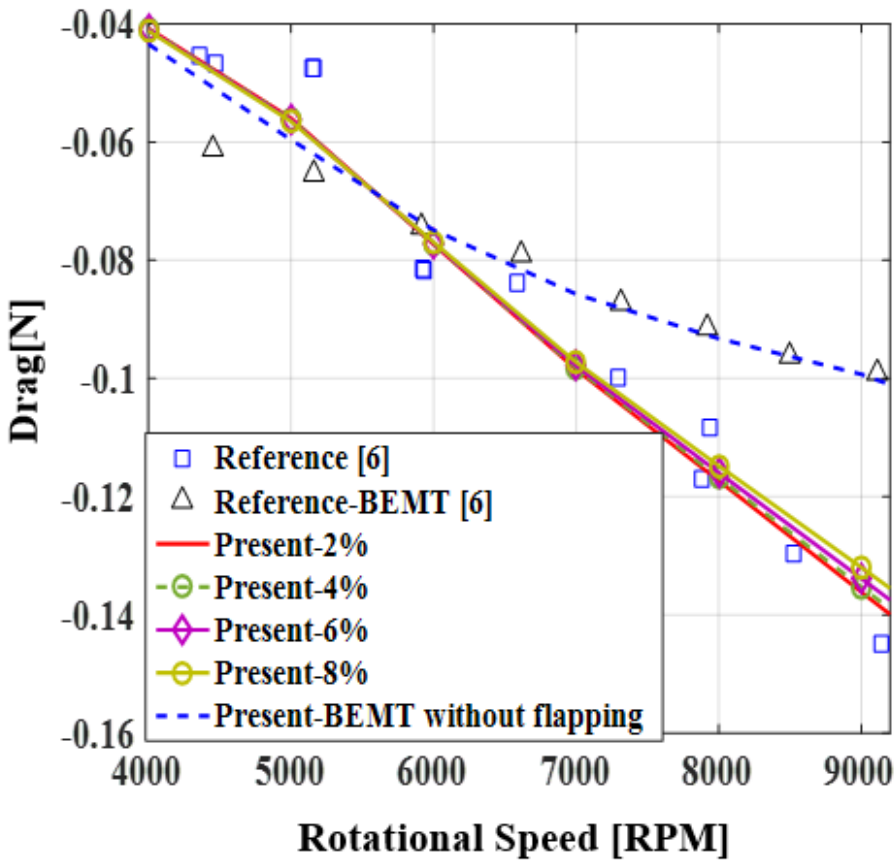

Fig. 3.9 Comparison of drag for each equivalent hinge offset position

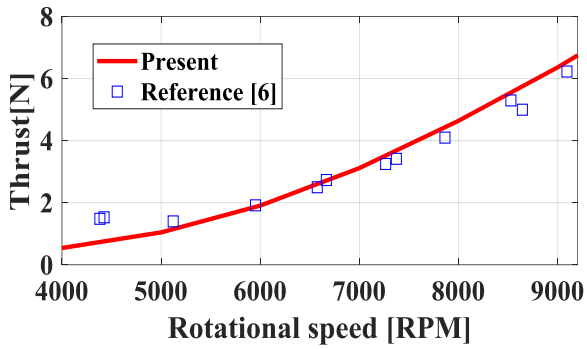

(a) Thrust (tilt angle = 0°)

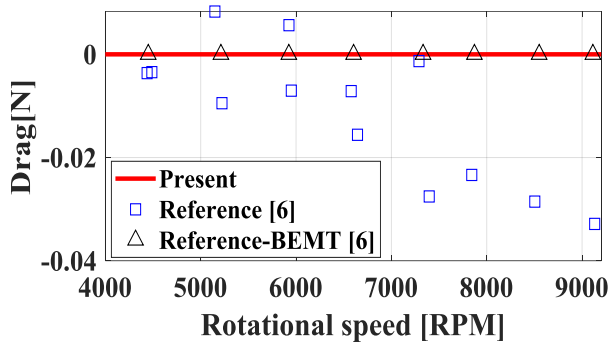

(b) Drag (tilt angle = 0°)

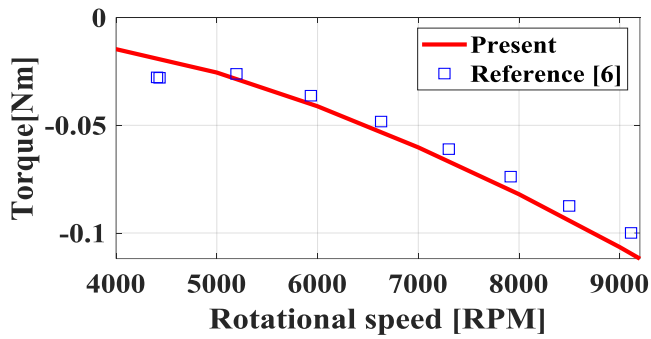

(c) Torque (tilt angle = 0°)

Fig. 3.10 Comparison between BEMT and experiment in forward flight for Graupner 9×5 (tilt angle = 0°)

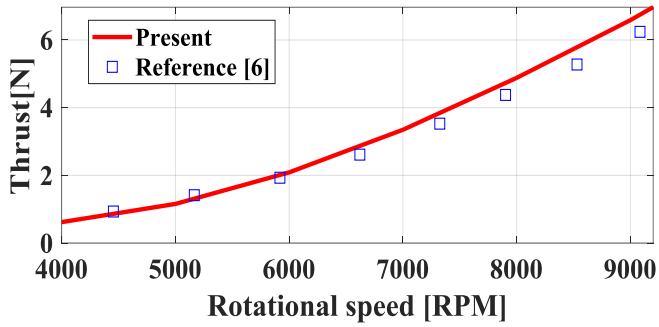

(a) Thrust (tilt angle = 30°)

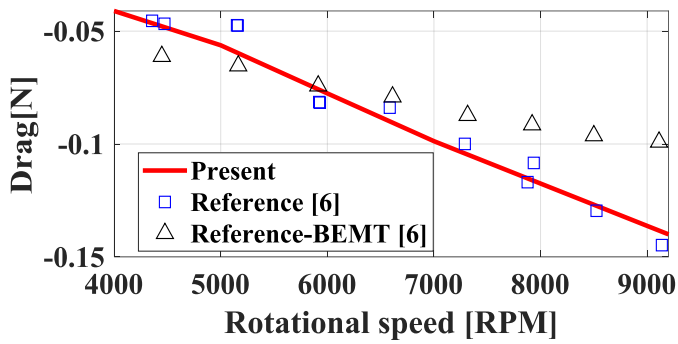

(b) Drag (tilt angle = 30°)

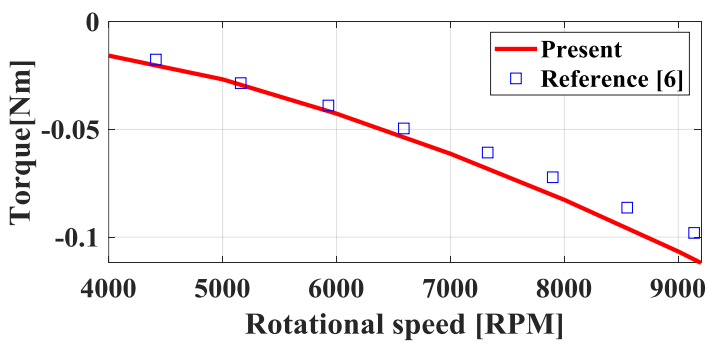

(c) Torque (tilt angle = 30°)

Fig. 3.11 Comparison between BEMT and experiment in forward flight for Graupner 9×5 (tilt angle = 30°)

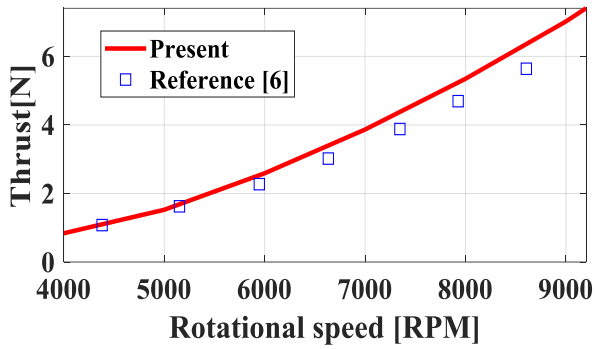

(a) Thrust (tilt angle = 60°)

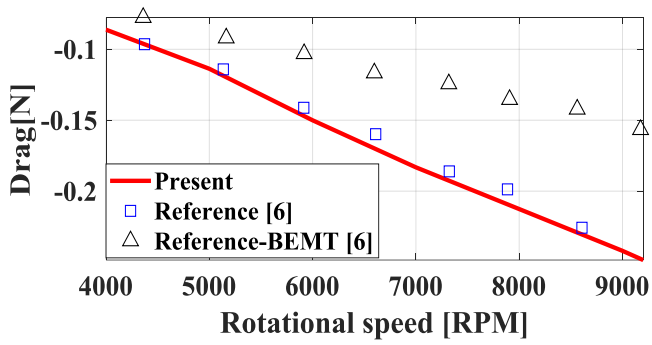

(b) Drag (tilt angle = 60°)

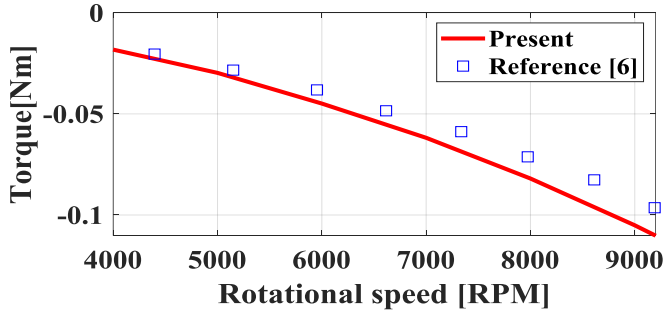

(c) Torque (tilt angle = 60°)

Fig. 3.12 Comparison between BEMT and experiment in forward flight for Graupner 9×5 (tilt angle = 60°)

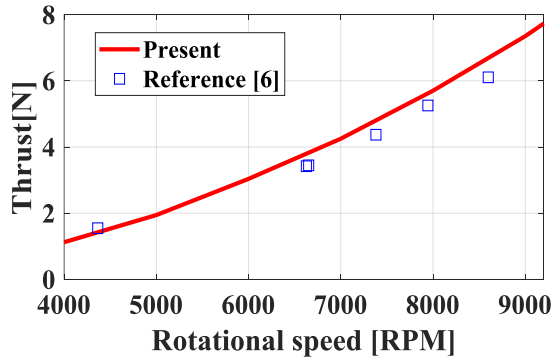

(a) Thrust (tilt angle = 90°)

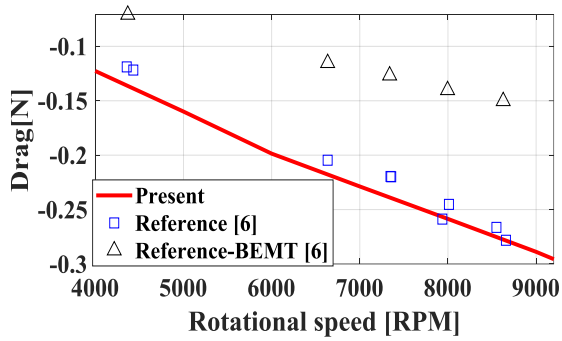

(b) Drag (tilt angle = 90°)

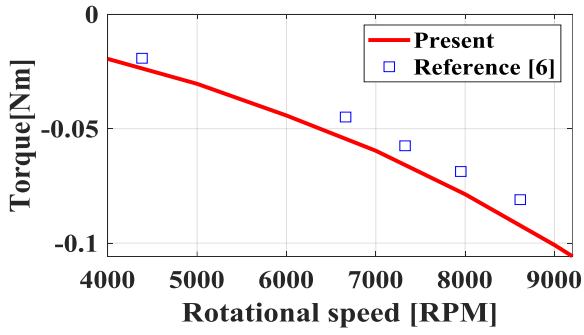

(c) Torque (tilt angle = 90°)

Fig. 3.13 Comparison between BEMT and experiment in forward flight for Graupner 9×5(tilt angle = 90°)

Table 3.1 Blade properties and rotation information at climb conditions

	APC 10 × 5	**APC 10 × 7**
Radius [in]	10	10
Number of blade [ea]	2	2
Rotational speed [RPM]	5000, 6000	5000, 6000
Airfoil shape	NACA 5521 NACA 4515 NACA 5512 NACA 4512 NACA 4511 NACA 4309	NACA 4521 NACA 5515 NACA 5513 NACA 4412 NACA 4411 NACA 4410 NACA 4309

3.3 Coupled Flight Dynamics Simulation Result

In this section, coupled analysis between the present BEMT and 6 DOF is performed. Since the flight test of DJI Matrice100 is not completed, the virtual UAV is utilized to assess prediction accuracy of the realistic flight. And using DJI hardware loop in simulation (HILS) system, system identification and parameter estimation are performed. That result will be shown later in Section 3.4.2. First, the indoor flight situation without gust is simulated using the virtual UAV, and it can be shown in Fig. 3.14. Comparisons are made between the one with and without BEMT. It is found that the time to reach the command altitude is longer than the one by the 6-DOF simulation without BEMT. When the realistic UAV is elevated, the thrust will be reduced under the same RPM. As it makes total thrust to reduce, response time to reach the altitude command is longer. It is seen that the result is comparatively well simulated. Eq. (3.4) consists of FAA gust profile[16], and the quadrotor is susceptible to either descending or rising winds.

$$\boldsymbol{V_{wind}} = \begin{Bmatrix} \boldsymbol{0 < x < d_m} \\ \frac{\boldsymbol{V_m}}{\boldsymbol{2}} \left(\boldsymbol{1 - cos}\left(\frac{\boldsymbol{\pi x}}{\boldsymbol{d_m}}\right)\right) \end{Bmatrix} \tag{3.4}$$

In Eq. (3.4), d_m is the travel distance, and V_m is the magnitude of each direction V_{mx}, V_{my},and V_{mz}. The gust is given as 2 m/s forward and 5 m/s upward. The results are shown in Fig. 3.15. As mentioned above, a quadrotor

is usually unstable, when the gust blows in either ascending or descending direction. The reason for such phenomenon is variation of thrust magnitude, and the quadrotor is easily perturbed by it. If gust blows in the upward direction, the rotor will become into the vortex ring state[14]. It cannot be analyzed by BEMT, but instead an empirical equation is commonly used. The present hybrid analysis uses the empirical equation which was suggested in Ref. 14. As a result, the phenomenon in which a quadrotor will experience under the gust will be analyzed. The results reveal that it possesses a capability of realistic flight simulation.

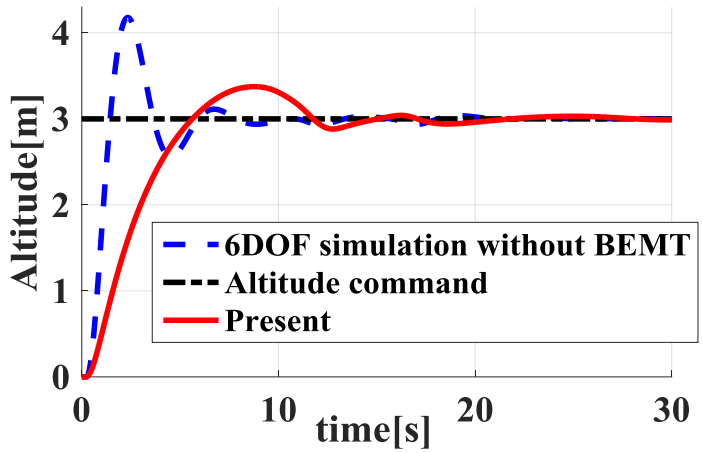

(a) Comparison of the altitude result

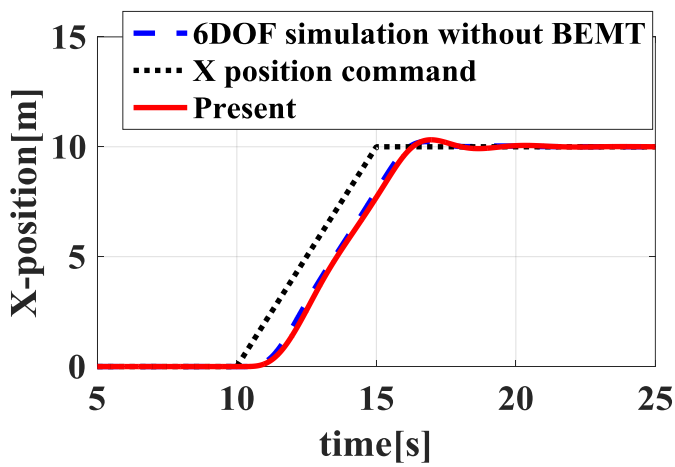

(b) Comparison of x position result

Fig. 3.14 Response by the altitude and global position input

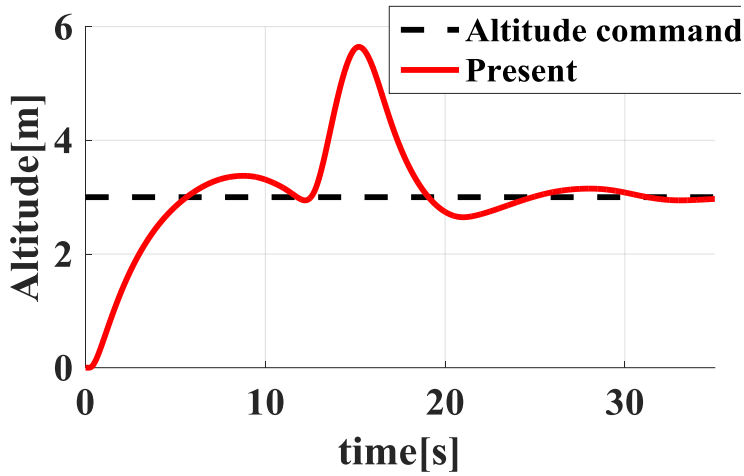

(a) Comparison of altitude result with gust

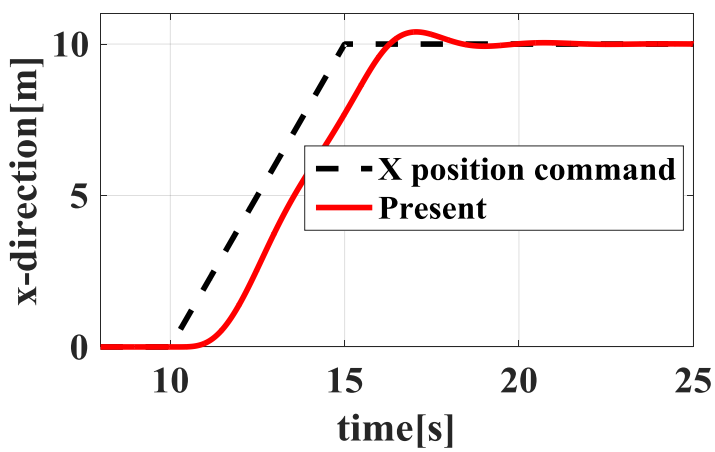

(b) Comparison of x position result with gust

Fig. 3.15 Predicted response due to the gust

3.4 Experiment Setting and Result

3.4.1 Individual Rotor Thrust Test

To understand the rotor characteristics of DJI Matrice100, information about the geometry and airfoil shape of DJI 1345T blade is required. Therefore, three-dimensional scanning is performed as in the previous studies [6-8], and the chord length, twist angle, sectional airfoil shape in the span direction are obtained. Chord length is already given in Fig. 2.4, and Fig. 3.16 shows the airfoil shape at the spanwise station 90% and built-in twist in terms of the radial station.

A static test facility is constructed as shown in Fig. 3.17. The test bed used in the static test bed is the '1580 series' product. As shown in Fig. 3.17, a side wall is installed in order to create a smooth stream. Thrust and torque obtained from Fig. 3.18 are verified by the present BEMT. As a result, as shown in Fig. 3.18, both thrust and torque result in discrepancy of smaller than 5%. However, it is possible to measure only thrust and torque by the test bed. When it is used in the wind tunnel test in the future, it will be difficult to measure drag. Thus a new type of an experimental facility is designed as shown in Fig. 3.19, and the wind tunnel test will be conducted.

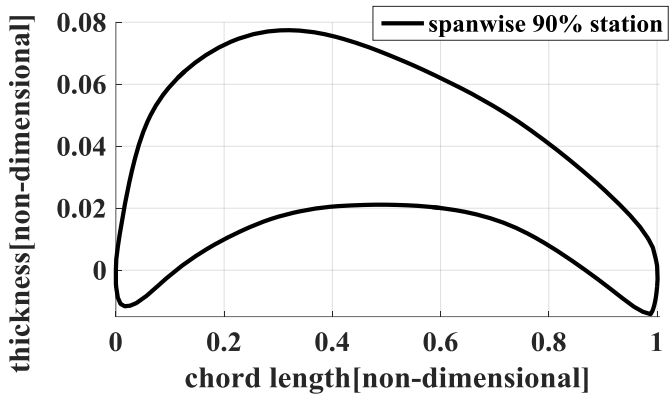

(a) blade section profile

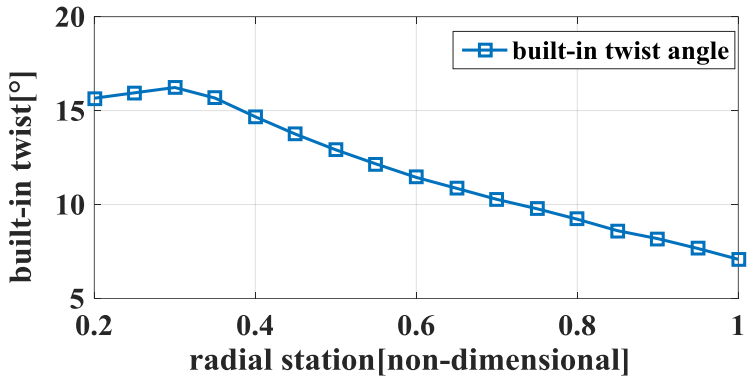

(b) built-in twist of DJI 1345T CW

Fig. 3.16 DJI 1345T CW blade configuration

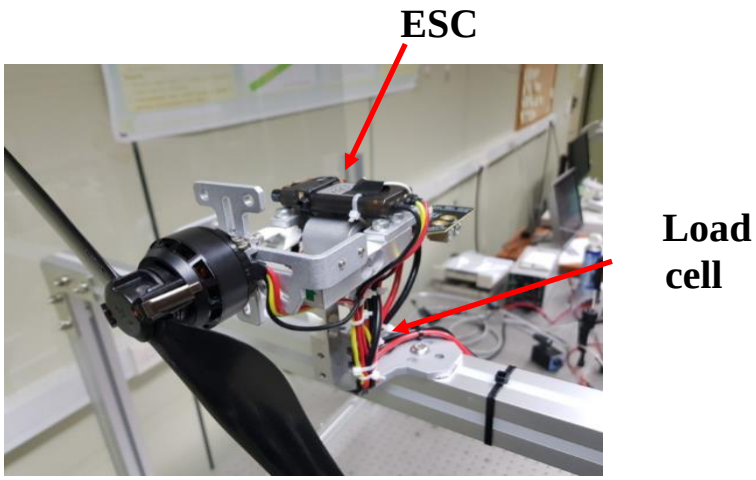

(a) front view

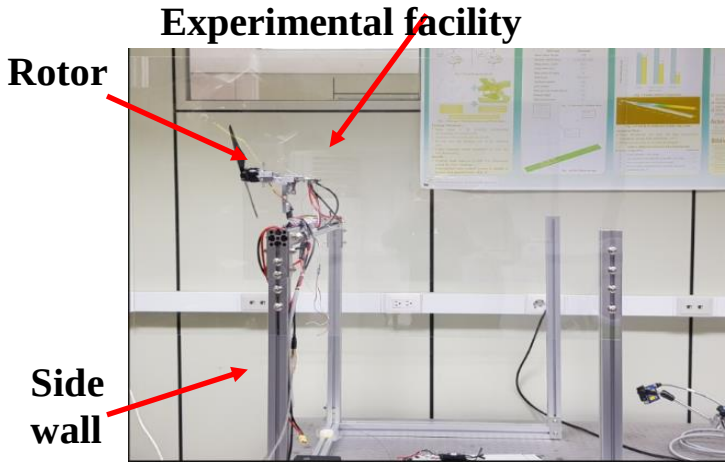

(b) rear view

Fig. 3.17 Present static experimental facility

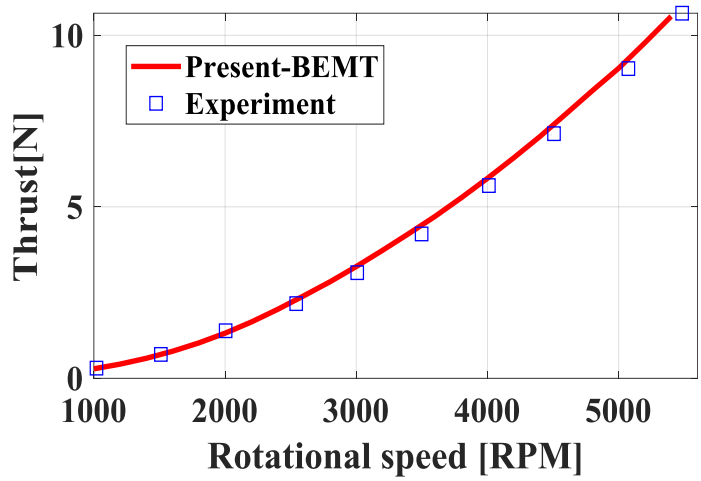

(a) Comparison of BEMT and experiment thrust

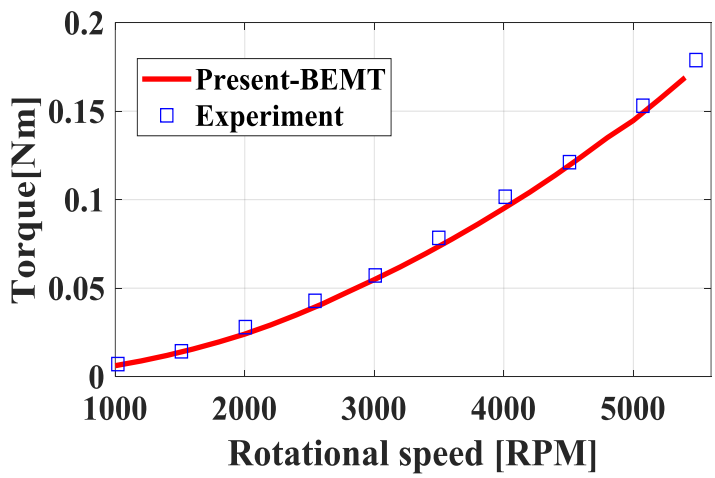

(b) Comparison of BEMT and experiment torque

Fig. 3.18 Comparison between BEMT and experiment in static condition for DJI 1345T CW

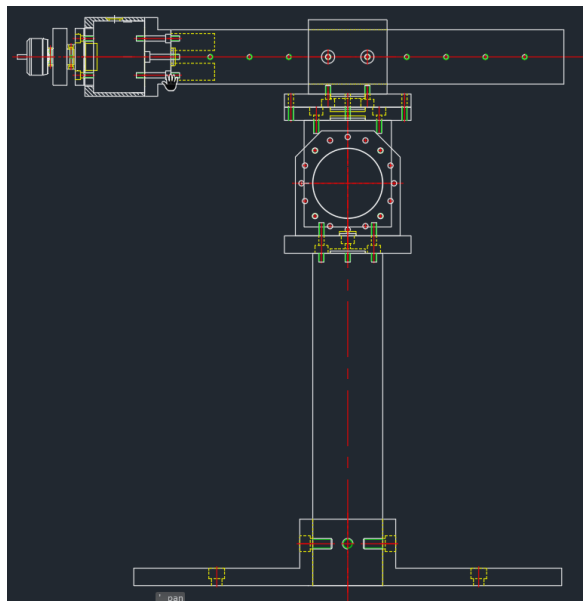

(a) Plane drawing of new type facility

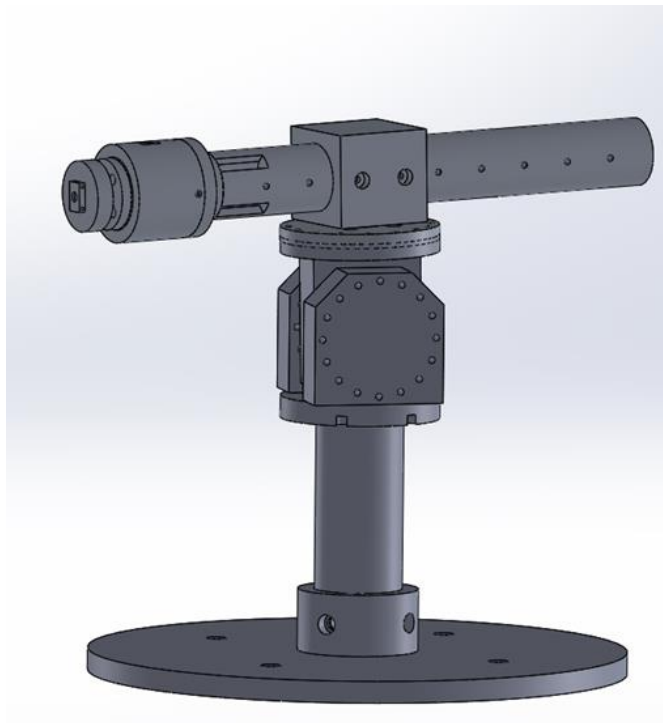

(b) CATIA drawing of new type facility

Fig. 3.19 New type facility for wind tunnel test

3.4.2 Hardware Simulation in Loop and Experiment setting for Flight Test

To control UAV and acquire data such as angle of UAV, angular velocity, translation velocity, and position, additional hardware setup is need. In this study, Manifold, which is made by DJI, is role of onboard computer and Manifold is using robot operating system(ROS). The total weight of DJI Matrice 100 is depend on additional equipment, but basic system weight is around 3kg. The code is based on DJI-SDK-ROS interface, and wifi is used for communicating labtop on ground station.

DJI supports user to check their own code using HILS system before test flight. As shown in Fig. 3.20, HILS system is constructed using DJI Matirce 100 & Manifold, and whole framework flow diagram is introduced in Fig. 3.21. To use this system, system identification and parameter estimation are conducted. The sin sweep code is based on Eq. (2.57), and this command can be directly inputted in roll, pitch, and yaw. The roll dynamics of DJI HILS is shown in Fig. 3.22. The roll dynamics gain is reduced and phase is delayed. The transfer function is derived from the single-input / single-output relationship using the decoupled dynamics assumed in this thesis. In this case, CIFER is used to obtain the transfer function. The estimation result is as shown in Fig. 3.23, and the model is estimated to be a zeroth-order numerator and second-order denominator system. Estimation results are confirmed by similarity between the DJI HILS system and the estimated model. The estimation transfer function is as follows.

$$G_{quad}(s) = \frac{53.8562}{s^2+9.7661s+51.8562} \quad (3.5)$$

Another method, steady-state sine method, is performed. The frequency range is 0.1 Hz to 1.1 Hz, and total simulation time for one set of frequency is 100 sec. This method is similar with previous method and Estimation output can be seen in Fig. 3.24. The estimation transfer function using this method is as follows

$$G_{quad_{steay}}(s) = \frac{51.94}{s^2+9.7661s+50.41} \quad (3.6)$$

From the results of Eq. (3.5) and (3.6), it is confirmed that the transfer function estimation method is reliable. In this case, the gain of the numerator is 1.05 times larger than the denominator. In this case, the steady-state error exists in Eq. (3.5) and (3.6). In order to facilitate the calculation of the parameter estimation, the steady value of the denominator and the gain value of the numerator are set to be the same.

To estimate PID controller gain of DJI Matrice 100, present simulation is compose as Fig. 3.25. First UAV properties is inputted auto trim module. The thrust to be generated by each motor according to the weight of UAV is calculated this module. It estimates the nominal RPM of the rotor for the control simulation. Moment of Inertia of UAV is referred by the other researchers [20].

The present simulation is compared with estimation transfer function conducted by CIFER in Fig. 3.26. Initial parameter values, which are controller

gain, are performed with the rule of thumb, one of the controller design methods. As shown in Fig. 3.26, it can be seen that the initial PID value shows a different response characteristic from the DJI transfer function. Therefore, it is performed to find the PID value that minimizes the cost function of Eq. (2.63), and the values are shown in Table 3.3. Through the verification of the DJI transfer function, the coupled 6 DOF simulation is confirmed to predict the controller gain of the black box using parameter estimation. Therefore, the data obtained from the flight test using the above-mentioned framework will be analyzed through a similar process. Through this, framework that enables comparison of flight and simulation in equal conditions is built.

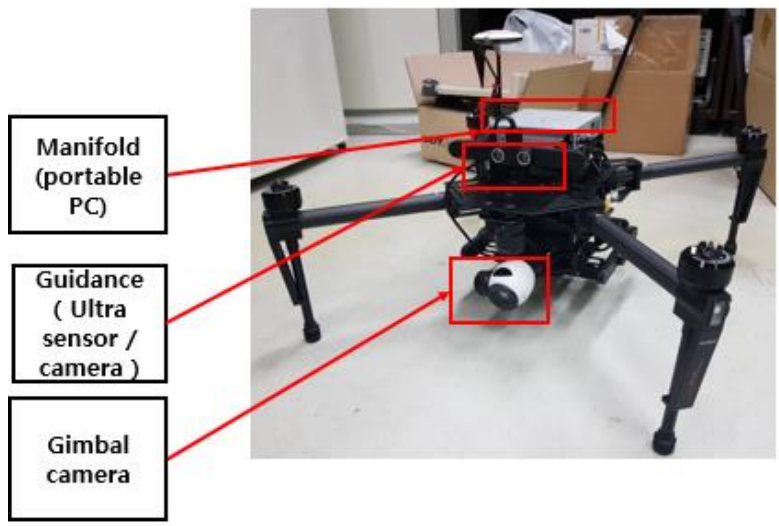

(a) Front view of DJI Matrice 100

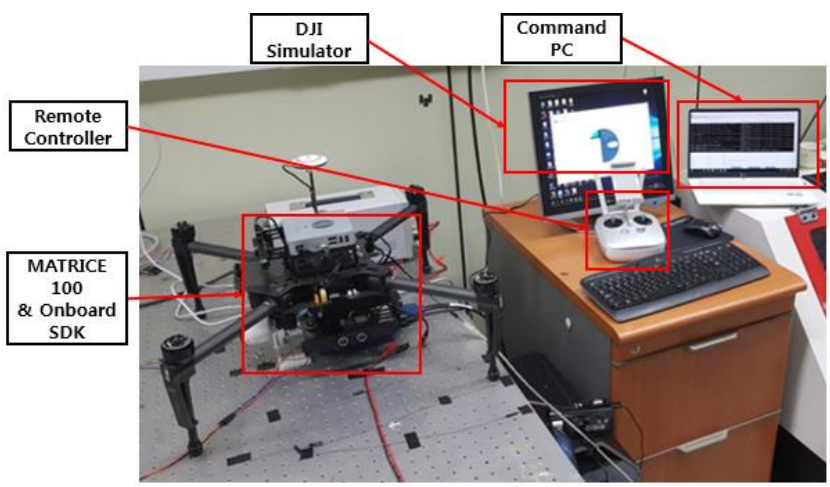

(b) Target UAV communication component

Fig. 3.20 DJI Matrice 100 HILS setup

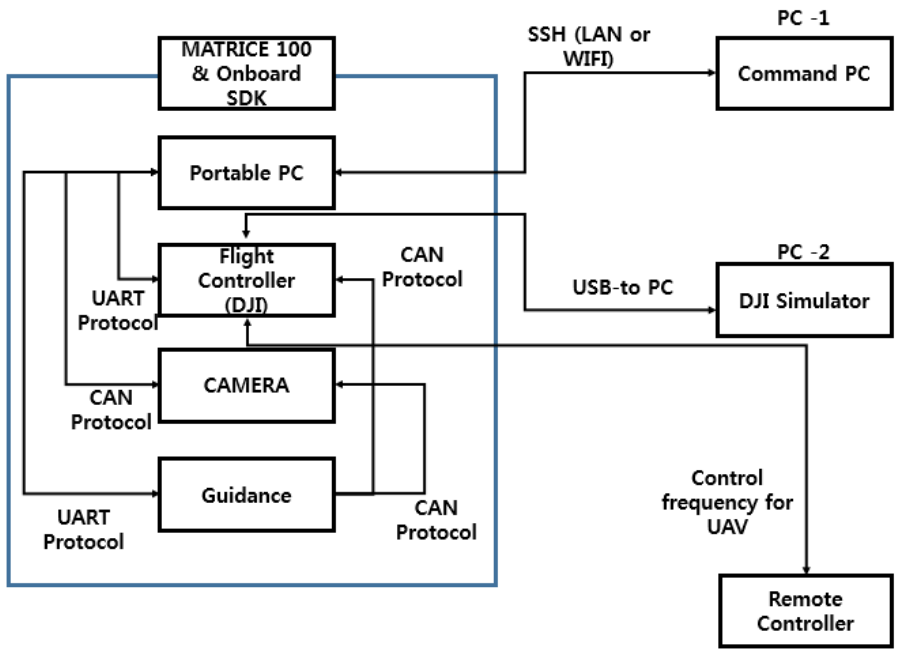

Fig. 3.21 HILS system of DJI

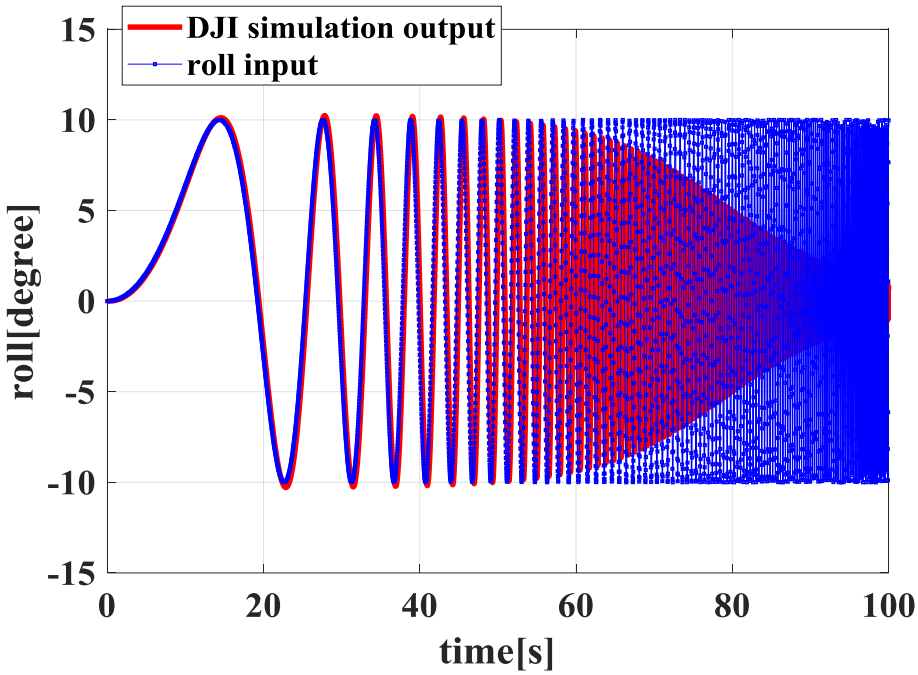

Fig. 3.22 Roll dynamics of DJI simulation

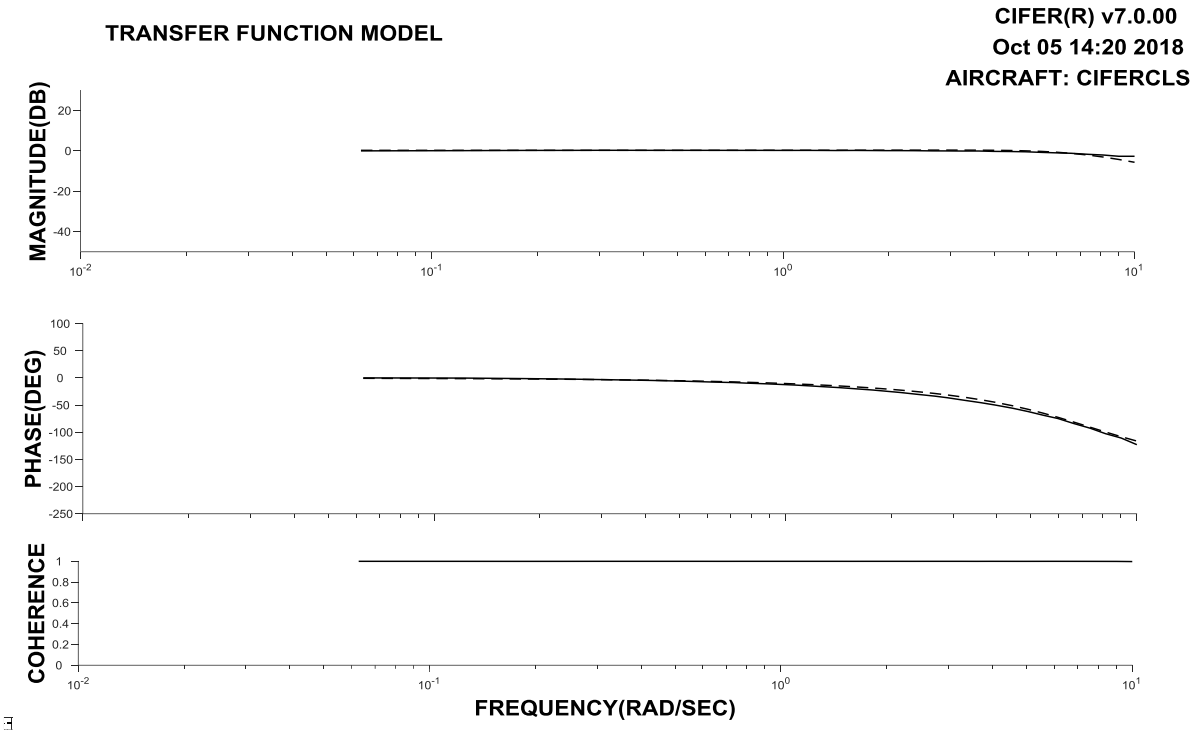

Fig. 3.23 CIFER estimation result

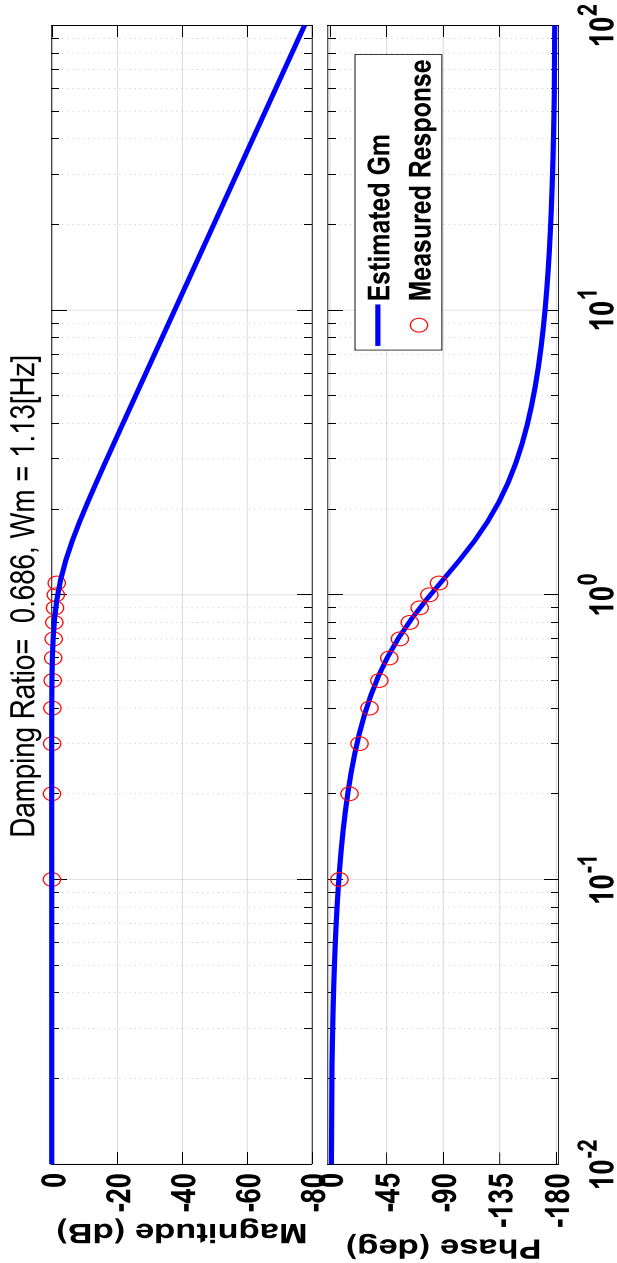

Fig. 3.24 Steady-state estimation result

Table 3.2 Moment of Inertia(MOI) DJI Matrice 100 [20]

I_{xx}	I_{yy}	I_{zz}
0.05535	0.05784	0.10667

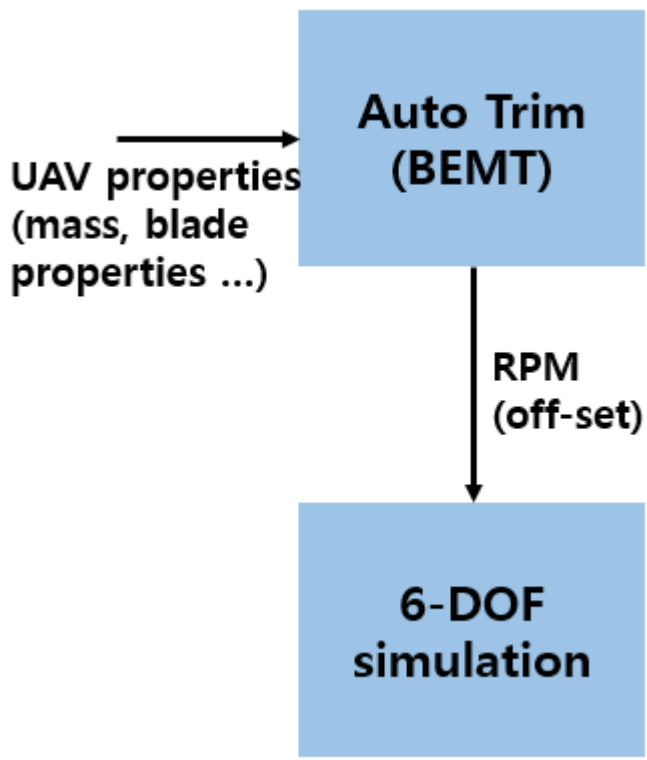

Fig. 3.25 Present coupled simulation flow

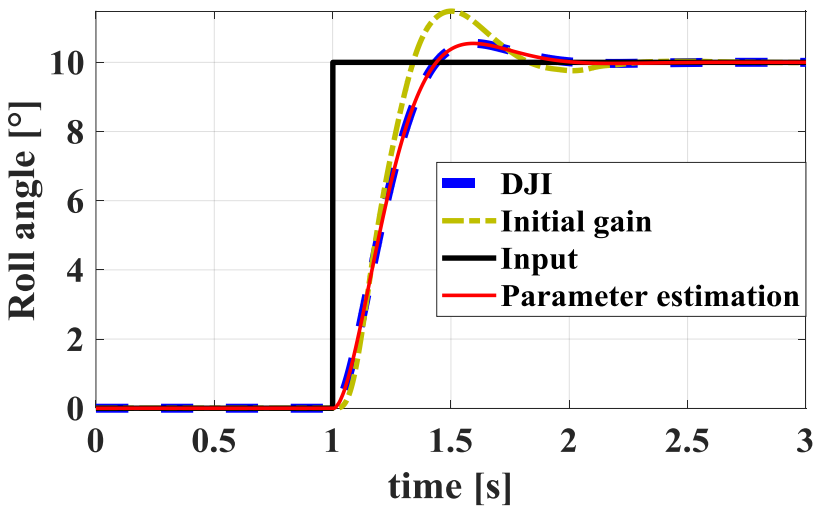

Fig. 3.26 Roll response

Table 3.3 Controller gain (roll)

	Initial gain value	Parameter estimation
Rate controller	$\mathbf{K_{d_r}}$ = 0.2176	$\mathbf{K_{d_r}}$ = 1.2368
	K_{p_r} = 8.7410	K_{p_r} = 391.3036
Attitude controller	$\mathbf{K_{p_a}}$ = 22.3357	$\mathbf{K_{p_a}}$ = 19.20
	K_{i_a} = 145.1737	K_{i_a} = 101.8
	K_{d_a} = 1.9500	K_{d_a} = 1

Chpater 4

Conclusion and Future Works

4.1 Conclusion

In this thesis, BEMT considering the gust and flight condition is developed. And coupled analysis between flight dynamics and the present BEMT is performed. By using CFD, reliability of the aerodynamic results obtained using XFOIL are ascertained. Experimental results under the hover, climb, and forward condition are compared with those by the present BEMT. In case of forward flight, BEMT considering the rigid blade flapping can predict the drag tendency more accurately. The average discrepancy between the present BEMT and the existing experiment results is smaller than 10%. In addition, three-dimensional scanning and hover experiment are performed, and compared with the present BEMT. The average discrepancy is smaller than 5%, when the static condition is analyzed. However, since this experiment zig doesn't consider drag of rotor, Additional equipment is designed and will be tested in various wind conditions in wind tunnel.

Based on these results, the present BEMT shows good agreement with the experiment. Hybrid analysis between flight dynamics and the present BEMT is established and the feasibility of the realistic flight simulation is evaluated by analyzing the effects of gust. The roll dynamics of the DJI HILS system is derived using system identification. The control gain of the controller which is

a black box is estimated by the parameter estimation method. The DJI Matrice 100 is equipped with an additional manifold to perform c++ coding to provide data acquisition and control commands during flight. It communicates with ground control laptop using wifi.

4.2 Future Works

In the future, it is necessary to evaluate the target blade, DJI 1345T, for each flight condition by wind tunnel test. Therefore, the wind tunnel test will be performed. Quadrotor UAV is unstable motion in vertical gust or vortex ring state condition. In addition, since preparation of flight experiment is ready, flight test will be performed. The interference relationship between the rotors will be tested and verified by flight test and wind tunnel using multi-rotor configuration. The attitude control and altitude control, which is the black box of DJI Matrice 100, through the flight experiment, will build a reliable simulation through it. The analysis about influence of UAV by gust will be carry out.

Reference

[1] Lee, D., Lim, H., Kim. H.J., Kim, Y., and Seong, K.J., "Adaptive Image-Based Visual Servoing for an Underactuated Quadrotor System," *Journal of Guidance, Control, and Dynamics*, Vol. 35, No. 4, 2012, pp. 1335-1353

[2] Johnson, R.D., *Unmanned Aircraft System Traffic Management (UTM) Project*, NASA Technical Report, TN-55386, 2018.

[3] Mellinger, D., Michael, N., and Kumar, Vijay, "Trajectory generation and control for precise aggressive maneuvers with quadrotors," *The International Journal of Robotics Research*, Vol 31, No.5, 2012, pp. 664-674.

[4] Hoffmann, G.M., Huang, H., Waslander, S.L., and Tomlin, C.J., "Quadrotor Helicopter Trajectory Tracking Control," *Proceedings of AIAA Guidance, Navigation and Control Conference and Exhibit, Guidance, Navigation, and Control and Co-located Conferences*, Honolulu, Hawaii, 2008

[5] Bansal, S., Akametalu, K,A., Jiang, F.J., Laine, F., and Tomlin, C.J., "Learning Quadrotor Dynamics Using Neural Network for Flight Control," *2016 IEEE 55th Conference on Decision and Control (CDC) ARIA Resort & Casino*, Las Vegas, USA, December 2016

[6] Theys, B., Dimitriadis, G., Hendrick, P., and Schutter, J.D., "Experimental and Numerical Study of Micro-Aerial-Vehicle Propeller Performance in Oblique Flow," Journal of Aircraft, Vol.54,

No.3, 2017, pp. 1076-1084

[7] MacNeil, R., and Verstraete D., “Blade element momentum theory extended to model low Reynolds number propeller Performance,” The Aeronautical Journal, Vol.121, No.1240, 2017, pp. 835-857

[8] Russell. C.R., Sekula, M.K., “Comprehensive Analysis Modeling of Small-Scale UAS Rotors”, 73rd AHS International Annual Forum and Technology Display, Fort Worth, TX, 2017

[9] McCrink, M.H., and Gregory, J.W., “Blade Element Momentum Modeling of Low-Re Small UAS Electric Propulsion Systems,” 33rd AIAA Applied Aerodynamics Conference, AIAA AVIATION Forum, Dallas, TX, 2015

[10] OL, M., and Zeune, C., “Analytical-Experimental Comparison for Small Electric Unmanned Air Vehicle Propellers,” 26th AIAA Applied Aerodynamics Conference, Honolulu, Hawaii, 2008

[11] Diaz, P.V., and Yoon, S., “High-Fidelity Computational Aerodynamics of Multi-Rotor Unmanned Aerial Vehicles,” NASA-ARC-E-DAA-TN49783, 2018

[12] Huang, H., Hoffmann, G.M., Waslander, S.L., Tomlin, C.J., “Aerodynamics and Control of Autonomous Quadrotor Helicopters in Aggressive Maneuvering,” IEEE Conference on Robotics and Automations, 2009, pp. 3277-3282

[13] Waslander, S.L.,“Wind Disturbance Estimation and Rejection for Quadrotor Position Control,” AIAA Unmanned...Unlimited Conference,

Seattle, Washington, 2009

[14] Leishman, J.G., Principles of Helicopter Aerodynamics, 2nd ed., Cambridge University Press, Cambridge, UK, 2006.

[15] Drela, M., "XFOIL: An analysis and design system for low Reynolds number airfoils," Low Reynolds Number Aerodynamics, Mueller, TJ, ed., Lecture Notes in Engineering, Vol. 54, 1989, pp. 1-12

[16] Transport Airplane Directorate, "AC 25.341-1 - Dynamic Gust Loads," ANM-115, 2014

[17] Shastry, A.K., Kothari, M., and Abhishek, A., "Generalized Flight Dynamic Model of Quadrotor Using Hybrid Blade Element Momentum Theory," Journal of Aircraft, published online 30 April. 2018. doi: 10.2514/1.C034899

[18] Brandt, J. B., "Small-Scale Propeller Performance at Low Speeds," M.S. Thesis, Department of Aerospace Engineering, University of Illinois at Urbana-Champaign, Illinois, 2005.

[19] Mark, B.T., Robert, K.R., *Aircraft and Rotorcraft System Identification Engineering Methods with Flight Test Examples*, AIAA Education Series, 2012

[20] Jeaong, H., Jo, S., Suk, J., Kim, S., Lee, Y., and Chung, I., "Modeling of Aerodynamic Database and Robust Control Using Disturbance Observer for Quadcopter", *Journal of Institute of Control, Robotics and Systems*, Vol 24, No.6, 2018, pp. 519-531.

[21] Anonymous, 'Estimate Parameters from Measured Data', Available:

https://kr.mathworks.com/help/sldo/gs/estimate-parameters-from-measured-data-using-the-gui.html#brj752_-1

국문초록

비행조건과 돌풍의 영향을 고려한 Blade Element Momentum Theory 와 쿼드로터형 무인 비행체의 동역학 결합 해석

박선후

서울대학교 대학원

기계항공공학부

무인비행체의 수요 및 공급이 증가하고 정찰, 감시, 택배등의 새로운 산업이 각광받고 있다. 이에 따라 무인비행체의 관련된 많은 기술들이 개발되는 실정이며 그 중에서도 가장 복잡하지 않은 형태인 쿼드로터 무인기가 많이 사용되고 있다. 이 무인기를 사용하여 도심지에서 택배 운송 혹은 정찰 등에 용이하게 쓰기 위해 카메라를 이용한 비전 알고리즘, 출 도착 알고리즘, 그 외의 많은 신기술들이 사용되고 있으나 도심지의 무인 비행체 운용여건상 건물 사이를 흐르는 측풍 이나 전단류 등에 의하여

추락할 위험성이 높다.

따라서 본 논문에서는 그러한 위험성을 해석하기 위해, 쿼드로터형 무인비행체의 공력 특성을 반영한 6 자유도 해석의 프레임워크를 구축하였다. 돌풍 및 비행 조건들을 고려하기 위해 바람의 좌표계 변환 개념을 제시하였으며, 강체 블레이드 플래핑 운동방정식을 고려한 깃 요소 및 운동량 이론을 이용해 개별 로터의 제자리, 전진, 상승 비행을 해석하였다. 또한 XFOIL 을 사용하여 공력 결과를 도출하였고 이를 전산유체역학 해석으로 검증하였다. 개발된 BEMT 를 이용하여 제자리, 상승, 전진 비행 조건에 대해 검증을 수행하였다. 또한 목표 기체인 DJI Matrice 100 의 블레이드의 삼차원 스캐닝을 수행하여 로터의 제자리 비행 특성을 비교 및 검증하였으며, 추가 풍동실험을 위해 실험장비를 설계하였다. 또한 DJI 에서 제공하는 HILS 시스템의 동특성 파악과 파라미터 추정을 통해 블랙박스 형태인 비행 제어기의 게인을 추정 가능한 6 자유도 시뮬레이션을 구축하였다.

주제어: 쿼드롭터, 깃 요소 및 운동량 이론, 강체 블레이드 플래핑 운동, 돌풍, 비행조건, 결합 해석

학번: 2017-28496